von KARMAN INSTITUTE
FOR FLUID DYNAMICS

Contract AF EOAR 66-6

Final Report

LAMINAR SEPARATION IN SUPERSONIC AND HYPERSONIC FLOWS

by

JEAN J. GINOUX

RHODE-SAINT-GENESE, BELGIUM

30 September 1966

DISCLAIMER NOTICE

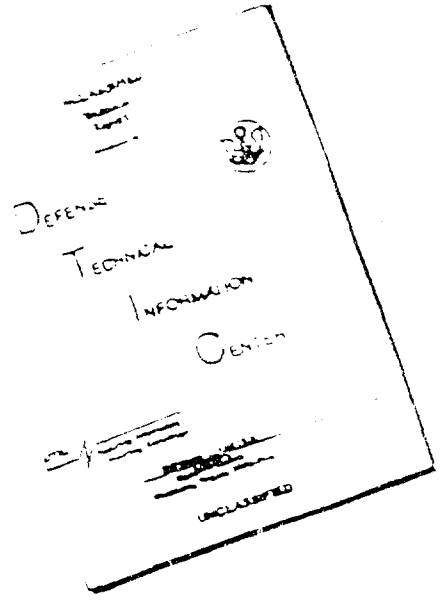

THIS DOCUMENT IS BEST QUALITY AVAILABLE. THE COPY FURNISHED TO DTIC CONTAINED A SIGNIFICANT NUMBER OF PAGES WHICH DO NOT REPRODUCE LEGIBLY.

Contract AF EOAR 66-6 30 September 1966

FINAL REPORT

LAMINAR SEPARATION IN SUPERSONIC AND HYPERSONIC FLOWS

1 OCTOBER 1965 - 30 SEPTEMBER 1966

JEAN J. GINOUX

von KARMAN INSTITUTE FOR FLUID DYNAMICS
Rhode-Saint-Genèse, Belgium

The research reported in this document has been sponsored by the Air Force Office of Scientific Research, O.A.R., through the European Office, Aerospace Research, United States Air Force.

TABLE OF CONTENTS

	Page
Summary	i
List of figures	ii
Symbols (Part I)	v
(Part II)	vi
Part I - Introduction	1
Equipment and models	2
Wind tunnel	2
Pressure measurements	2
Thermal measurements	2
Sublimation technique	3
Models	4
Results and discussion	6
Pressure measurements	7
Recovery temperatures (natural transition)	8
Recovery temperatures (artificial transition)	11
Heat transfer measurements	12
Conclusions	14
Part II - Introduction	16
Equipment and models	17
Wind tunnel	17
Heat transfer measurements	17
Models and injection system	18
Results and discussion	19
Conclusions	21
References	

SUMMARY

Static pressure, recovery temperature and heat transfer distributions have been measured on flat plates with flaps at a Mach number of 2.02. A uniform amount of heat was dissipated at the surface of the models. The angle of the flaps was varied between 1.5° and 21°. Laminar, transitional, and turbulent flows were considered.

Well defined plateau pressures existed when reattachment was transitional and not in fully laminar flows. A large peak of recovery temperature existed, when transition was in the reattachment zone, followed by fairly low recovery temperatures. Heat transfer results generally agreed with other measurements made with isothermal walls. No peak of heat transfer was detected in the reattachment region.

Heat transfer distributions have been measured at a Mach number of 6.7 on a cone-cavity model with air injection into the separated flow region. The mass injection rate was varied between zero and a maximum equal to the mass flow in the boundary layer at separation.(Q_{BL}). The effect of injection was to considerably reduce the heat transfer rate to the cavity floor and in the reattachment region of the flow.

At an injection rate of about 0.25 Q_{BL}, the heat transfer was found to be reduced below the cone values over the whole surface of the body. At higher rates of injection, transition moved forward with correspondingly larger heat rates.

LIST OF FIGURES

Figure 1

a, b. Shadowgraphs of the flow around a 5-deg. flap
a: $R_e=1.5\times10^6$ m^{-1} b: $R_e=2.2\times10^6$ m^{-1}

c, d. Shadowgraphs of the flow around a 7-deg. flap
c: $R_e=1.5\times10^6$ m^{-1} d: $R_e=3.0\times10^6$ m^{-1}

e, f. Shadowgraphs of the flow around a 10 deg. flap
e: $R_e=1.5\times10^6$ m^{-1} f: $R_e=3.0\times10^6$ m^{-1}

g, h, i. Shadowgraphs of the flow around a 15-deg. flap
g: $R_e=1\times10^6$ m^{-1} h: $R_e=1.5\times10^6$ m^{-1}
i: $R_e=3.0\times10^6$ m^{-1}

j, k. Schlieren photographs of the flow around a 21-deg. flap
j: $R_e=1.5\times10^6$ m^{-1} k: $R_e=3.0\times10^6$ m^{-1}

l, m, n. Schlieren photographs of turbulent flows around flaps at $R_e=3.0\times10^6$ m^{-1}
l: $\theta=10°$ m: $\theta=15°$ n: $\theta=21°$

Figure 2

a. Heat transfer distribution over a 1.5-deg. ramp (model CCA4)

b. Pressure and heat transfer distributions on a 3-deg. ramp (models CC4 and CCA3)

c. Pressure and heat transfer distributions on a 5-deg. ramp (models CC5 and CCA5)

d. Static pressure distribution on a 7-deg. ramp (model CC7)

e. Pressure and heat transfer distributions on a 10-deg. ramp (models CC6 and CCA1)

f. Pressure and heat transfer distributions on a 15-deg ramp (models CC9 and CCA6)- Natural transition

g. Pressure and heat transfer distributions on a 15-deg. ramp (models CC9 and CCA6) - Turbulent flow

h. Heat transfer distribution on a 21-deg flap (model CCA7)

Figure 3 - Summary of the static pressure distributions for various flap angles

a- $R_e = 1.5\ 10^6\ m^{-1}$

b- $R_e = 3.0\ 10^6\ m^{-1}$

Figure 4 - Temperature distributions over the flap models

a- $\theta = 1.5°$

b- $\theta = 3°$

c- $\theta = 5°$

d- $\theta = 10°$

e- $\theta = 15°$

f- $\theta = 21°$

Figure 5- Summary of the recovery temperatures for various flap angles

a- $R_e = 1.5 \times 10^6\ m^{-1}$

b- $R_e = 3.0 \times 10^6\ m^{-1}$

Figure 6 - Effect of unit Reynolds number on recovery temperature distribution for a flap angle of 10 degrees.

Figure 7- Sublimation pictures of the flow around a 10-deg. flap

a- $R_e = 1.5 \times 10^6\ m^{-1}$

b- $R_e = 3.0 \times 10^6 m^{-1}$

Figure 8 - Effect of transition location on the recovery temperature distribution for a flap angle of 15 degrees.

Figure 9 - Recovery temperature distributions for fuily turbulent flows at various flap angles.

Figure 10 - Summary of the heat transfer results for laminar and transitional flows.

a- $R_e = 1.5 \times 10^6\ m^{-1}$

b- $R_e = 3.0 \times 10^6\ m^{-1}$

Figure 11 - Summary of the heat transfer results for turbulent flows over flap models.

Figure 12 - Cone-cavity model for gas injection studies at hypersonic speeds.

Figure 13 - Effect of mass injection on heat transfer distribution over a cone cavity model at M = 6.7.

Figure 14 - Effect of mass injection on heat transfer distribution over a cone cavity model at M = 6.7.

SYMBOLS

c_p Specific heat at constant pressure

h Heat transfer coefficient; $h=q/(T_w-T_r)$

k_e Heat conductivity coefficient

L Length of flap

M_c Mach number upstream of interaction region (M_e=2.02)

M_f Mach number at infinity downstream on the flap

N_u Nusselt number = hk_e/x

p Local static pressure

p_e Static pressure upstream of interaction region

p_o Stagnation pressure

q heat flux per unit area and unit time, dissipated uniformly at the surface of the models (cal/m^2 sec)

R_e Unit Reynolds number in the flow parallel to the flat plate upstream of interaction region; $R_e = \frac{U_e \rho_e}{\mu_e}$ (m^{-1})

R_{ex} Reynolds number based on local distance x; $R_{ex}=xR_e$

R_{ex_o} Reynolds number based on distance x_o; $R_{ex_o}=x_oR_e$

S Model span

T_o Stagnation temperature

T_r Recovery temperature

T_w Wall temperature with uniform heat flux

x Streamwise coordinate measured from the leading edge along the surfaces of the plate and of the flap.

x_o Distance between the leading edge of the model and the point where the interaction is first felt

x_t Distance between the leading edge of the model and transition

μ_e Viscosity coefficient upstream of interaction

ρ_e Density upstream of interaction

θ Flap angle

SYMBOLS (PART II)

c	Specific heat of the skin material
c_q	Rate of injection = Q/Q_{BL}
d	Thickness of the skin
q	Heat transfer rate with mass injection
q_o	Heat transfer rate without mass injection
q_c	Heat transfer rate on a simple cone
Q	Mass injected per unit time
Q_{BL}	Mass flow in the boundary layer at separation
t	Time
T	Temperature
x	Coordinate along cone (see figure 12)
ρ	Density of skin material

PART I

INTRODUCTION

In the course of previous investigations on separated flows made by the author (1, 2, 3), it was shown that regular and strong streamwise vortices developed systematically in laminar reattaching boundary layers at supersonic and hypersonic speeds. Although the main body of the research was made with backward facing steps, the phenomenon was also observed in other types of reattaching flows and, in particular, in separated flows over ramps or control surfaces. Such vortices were shown to cause spanwise variations of the heat transfer rate at and downstream of reattachement with local peaks higher than the known turbulent flow values. However the mean heat transfer rate, i. e. the average over a portion of the span large compared to the spacing of the vortices, was not appreciably affected by the vortices.

When this phenomenon was qualitatively observed in the reattaching flow over a 10-deg. flap, with a sublimation technique, regular striations patterns appeared as usually observed by the author in other types of separated flows. However the average rate of sublimation was surprisingly high at reattachment. Although this could have been explained by the existence of a peak of heat transfer in that region, as observed by other investigators in reattaching flows, it was in order to make a direct verification of this fact. Preliminary tests, made on such a flap model, showed that there was no such peak (4) but rather that a maximum of the recovery temperature existed in the reattachment region which had not been reported before. It was then decided to study this phenomenon in a more systematic manner. This report is related to the results of such an investigation.

The research reported in this document has been sponsored by the Air Force Office of Scientific Research, O. A. R., through the European office, Aerospace Research, United States Air Force, under Grants AF. EOAR 65-11 and 66-6.

EQUIPMENT AND MODELS

Wind Tunnel

The tests were made in the VKI 16" x 16" continuous supersonic wind tunnel at a Mach number of 2.21, over a range of stagnation pressures from 100 mm Hg (i.e. 1.8 psi) to 200mm Hg (3.6 psi) absolute which corresponds to free stream Reynolds numbers of $1.5\ 10^6$ and 3×10^6 per metre respectively.

The stagnation temperature is of about 15°C to 30°C (59°F to 86°F) depending upon the stagnation pressure. At a given pressure level, it increased gradually during a test at a rate of 1 to 2°C per hour.

The tunnel is equipped with shadow and single pass schlieren systems with parabolic mirrors. Pictures are taken with a spark light source of a few micro-seconds duration time.

Pressure Measurements

The static pressure distributions were measured with 0.5 and 1.0 psi strain gage transducers and scanning valves located inside the tunnel circuit. The output of the transducers was recorded by a four digit digital voltmeter. Calibrations were made before and after each test to within $\pm$ 0.2 mm Hg.

Thermal Measurements

The recovery temperatures and heat transfer rates were measured with a steady state technique developped by the author (5).

Models are made of an insulating material (araldite) and covered with thin film of silver of nearly constant thickness (one micron thick plus or minus ten percent). Heat can thus be uniformly dissipated at the surface of the models by the Joule effect in the silver films and the heat flux per unit area (9) can be computed from the ratio of the product, current times voltage, to the area covered by the silver film. Heat losses

to the interior of the model are minimized by a symmetric design of the model. Thermocouples, installed flush with the surface along the center-line of the model , are used to measure the recovery temperature T_r (i.e. when q=0) and the wall temperature T_w with uniform heat dissipation ($q \neq 0$) . The heat transfer coefficient (h), the Stanton number (S_t) and the Nusselt number (N_u) are then calculated from:

$$h = \frac{q}{T_w - T_r} \quad , \quad N_u = \frac{hk_e}{x} \quad , \quad S_t = \frac{h}{\rho_e U_e C_p}$$

where subscript (e) is related to the flow parallel to the model surface, upstream of the interaction region.

Thermal equilibrium is generally achieved after one to one and a half hour of running time.

Thermocouples were made of copper-constantan wires 0.1 mm in diameter and calibrated before and after the tests to within $\pm$ 0.2°C.

The total amount of heat dissipated at both the upper and lower surfaces of the models were generally small , about 50 watts, thus giving values of q of the order of 0.1 cal/m^2.sec. The driving temperatures $T_w - T_r$ were accordingly small , with maximum values of about 30 to 50°C and minimum values (downstream of reattachment at large flap angles) of 5°C. However , the accuracy of the measurements is believed to be good, because errors are eliminated by taking the difference between T_w and T_r measured by the same thermocouples during the same test. With small values of q , quasi-adiabatic conditions were reached which means that the flow was not affected by the transfer of heat. This was verified by measuring the pressure distribution on model CCA2 with and without heat dissipation at the model surface. No difference was found.

Sublimation Technique

The flow near the surface of one of the models was visualized by using a sublimation technique with acenaphthene as an indicator. The model was first sprayed with tracing blue ink , to increase the contrast, and then

with the indicator whose thickness was such that a running time of one to two hours was needed to obtain the surface pattern. On the photographs (fig. 7) included in this report, darker regions are representative of larger sublimation rates than brighter ones.

Models

Two types of models were used ; metallic ones (CC-series) for pressure measurements and those made of araldite (CCA-series) for thermal measurements. A different model was made for each flap angle.

The designation of the models and their main dimensions are given in Table 1, where θ is the flap angle in degrees, S the model span and L the length of the flap in millimetres. On all the models, the flat plate upstream of the flap was 120 mm long and was inclined by 5 degrees in the test section. The effective Mach number (M_e) was thus 2.02. This inclination was necessary to ensure complete symmetric flow condition, when both the upper and lower surfaces of the araldite models were heated up at the same rate.

TABLE 1

Model	θ (degrees)	S (mm)	L(mm)
CCAI	10	250	120
CCA2 *	10	250	120
CCA3	3	250	120
CCA4	1.5	250	120 (+50)**
CCA5	5	250	120 (+50)**
CCA6	15	386	100
CCA7	21	386	70 (+25)**
CC4	3	250	120
CC5	5	250	120

CC7	7	250	120
CC6	10	250	120
CC9	15	386	125

* with static pressure orifices
** additional after body with surface parallel to tunnel free stream

Araldite models were cast after installing the thermocouples and the electric wires in the mould. They were made of araldite type D except model CCA7. Araldite D is simpler to use but the maximum wall temperature is limited to 40 to 60°C (100 to 150°F). For large flap angles the maximum temperature is reached, with uniform heat flux, in the separated flow region where S_t is smaller, while T_w remains rather low in the reattachment region of the flow. The driving temperature $(T_w - T_r)$ can thus be rather small with a corresponding increase in the inaccuracy of the heat transfer measurements. For this reason, one of the models (CCA7) was made of araldite F which can be used at higher temperatures before warping.

A special araldite model (CCA2) was made with a 10-deg. flap which contained a limited number of both pressure taps and thermocouples, to verify the effect of heat transfer on the pressure distribution as mentioned in describing the technique of heat transfer measurement.

To check the effect of heat conduction inside the model, model CCA6 was remade with a hollow flap such that only a thin skin of araldite, 0.3 mm thick and 25 mm wide, existed all along the centerline of the flap. Thermocouples were embedded in that thin skin. No heat conduction effect was found.

The araldite models were machined after casting, but their leading edges were not as nice as on the metallic ones. To check the effect of leading edge irregularities, a comparison was made of the pressure distributions on models CCA2 and CC6. In another test, artificial roughness were placed at the leading edge of model CCA2, and the pressure

and heat transfer distributions were measured . There was no indication within the accuracy of measurements of a leading edge effect.

RESULTS AND DISCUSSION

The result of static pressure and heat transfer measurements are presented and discussed in the following sections. The flap angle was varied from 1.5 to 21 degrees and two stagnation pressure levels were used, i.e. 100 and 200 millimetres of mercury corresponding to unit Reynolds number of $1.5\ 10^6$ and $3\ 10^6$ per metre in the flow parallel to the flat plate.

Flow Visualization

Shadowgraphs or schlieren photographs of laminar, transitional and turbulent flows over flaps of various angles are shown in figures 1 - (a to n). Turbulent flow is obtained artificially by tripping the boundary layer upstream of the flap with a paper strip, 10 mm wide and 1.4 mm thick, covering the whole span of models and located 20 mm downstream of the nose of the models.

Pictures of the flow over 1.5 and 3 deg. ramps are not shown because they are similar to those given in figures 1a and 1b for the 5-deg. flap.

For a 5-deg. ramp, the flow is laminar over the whole model. The flow is on the verge of separation as shown by the pressure distribution.

For θ=7degrees, the flow is separated and transition appears, at the highest free stream Reynolds number , far downstream of reattachment.

For θ= 10 and 15 degrees, transition has moved closer to or in the reattachment zone and finally at θ = 21 degrees, transition is located upstream of reattachment.

Table II gives the distance x_t of transition from the model leading edge as measured on photographs of figure 1, for θ = 10, 15 and 21 degrees, for the two stagnation pressure levels (100 and 200 millimetres of mercury.).

TABLE II

θ degrees	p_o mmHg	x_t mm
10	100	170-200
	200	140-150
15	100	150
	200	135
21	100	105-110
	200	95-100

With the roughness element, the flow remained attached on the 10 and 15 deg. flaps. For θ=21 degrees, oil flow visualization showed a region of reversed flow starting approximatively 10 mm upstream of the nose of the ramp.

Pressure Measurements

The ratio p/p_e is plotted versus x in figures 2b to 2g for two stagnation pressure levels (I00 and 200 mm Hg) corresponding to unit Reynolds numbers , in the flow parallel to the flat plate, of $1.5\ 10^6$ and $3.0\ 10^6$ respectively. p is the local static pressure, p_e the static pressure upstream of the interaction region and x the distance , in millimetres, from the leading edge of the model, measured along the flat plate and the flap surfaces. These results are summarized by the curves of figures 3a and 3b.

Flow separation occurs at a flap angle of about 5 degrees as indicated by the presence of a kink in the pressure distribution for θ =5 degrees. A plateau of nearly constant pressure develops for a flap angle larger than 7 degrees. From the flow pictures previously discussed, transition was observed in the reattachment region in these conditions. Therefore, there does not seem to exist , at least within the present tests conditions, a fully

laminar separated flow with a well defined plateau pressure as is generally assumed in the literature (6, 7, 8) . The sensitivity of the present flows to the transition location will appear more fully when discussing the results of the thermal measurements.

The plateau pressures for the "transitional flows" are compared with Chapman's formulae (9) established for laminar flows:

$$p_{sh} = p_e \left[1 + \frac{1.24\, M_e^2}{\left[(M_e^2 - 1)\, R_{ex_o} \right]^{1/4}} \right]$$

where R_{ex_o} is the Reynolds number based on conditions upstream of the interaction zone and x_o the distance between the leading edge of the model and the point where the interaction is first felt. A good agreement is obtained as indicated in figures 3a and 3b, showing that the presence of transition in the reattachment zone does not influence, as expected, the free interaction region located near separation.

The pressure distribution region for turbulent flow is shown in figure 2g for a flap angle of 10 degrees and a stagnation pressure of 200 mmHg. The upstream influence of the flap is very small and there is no indication of flow separation.

The total pressure rise is in good agreement with the inviscid theory with a tendency for overshooting in all three types of flows.

Recovery Temperatures (Natural Transition)

The distributions of recovery temperature (adiabatic wall) measured along the centerline of the models are plotted in figures 4a to 4f in degrees centigrade, for various flap angles and for the two free stream unit Reynolds numbers 1.5×10^6 and 3.0×10^6 per metre. Temperatures are shown rather than recovery factors, because of the uncertainty in the calculation of the static temperature distribution in the outer stream . The measured tempera-

-tures have been multiplied by the ratio of a reference stagnation temperature of 300°K (i.e. 27°C) over the actual stagnation temperature measured in each test. This reference level is indicated in the figures as well as the corresponding theoretical values of the recovery temperatures on a flat plate based on the initial Mach number (M_e) of 2.02 and also on the final Mach number (M_f), function of the flap angle. The laminar values are based on a recovery factor of 0.85 while the turbulent ones are based on 0.90.

These results are summarized in figures 5a and 5b for flap angles between 5 and 21 degrees, by smooth curves drawn through the experimental points.

For $\theta \leq 5°$, the recovery temperature increases gradually through the interaction region, from the flat plate laminar flow value at the initial Mach number to the corresponding value at the final Mach number. This is in agreement with the flow pictures which show fully laminar flows.

For a flap angle of 10 degrees, a very interesting result is obtained. At the lowest unit R_e number, for which transition is located downstream of the reattachment region, the recovery temperature increases smoothly, as expected, from the laminar flat plate value to the turbulent one, possibly followed by a slight decrease. However at the highest Reynolds number, which corresponds to a transitional reattachment, the recovery temperature increases more rapidly, reaches a peak at $x = 140$ mm and then decreases rapidly down to a value which is roughly the turbulent value on a flat plate at the initial Mach number rather than the final one.

Figure 6 shows the gradual modification of the recovery temperature distribution with increasing Reynolds number. The temperature peak increases and moves upstream, while the downstream temperature decreases as the Reynolds number increases. At the same time, the reattachment point as well as transition moves upstream. It seems from the flow pictures that transition was approximatively located at the

temperature peak. It is also observed that the temperature distribution did not vary upstream of the nose of the flap as R_e varied.

For a flap angle of 15 degrees, a peak existed in the recovery temperature distribution over the whole range of Reynolds number. Figure 5b shows that this peak is higher than on the 10 deg. flap while the recovery temperature drops, downstream of reattachment, to a lower value (even lower than the laminar flat plate value based on the final Mach number). Comparison with the flow pictures seems to indicate that transition is located slightly downstream of the temperature-peak at both unit Reynolds numbers.

For a flap angle of 21 degrees, the temperature peak is still present although flatter and located this time, like transition, upstream of the nose of the ramp and also, of course, of reattachment. The final temperature downstream of reattachment is again fairly low compared to the theoritical turbulent flow value at the final Mach number of 1.17. It is also observed from the figures that a second , although weaker, peak existed in the reattachment region at the lowest Reynolds number.

Figures 7a and 7b give the sublimation pictures of a 10-deg. flap model at unit Reynolds number of 1.5×10^6 and 3.0×10^6. At the lowest R_e, a striation pattern exists which is characteristic of laminar reattaching flows and their associated streamwise vortices (1). At the highest R_e, striations are still present but there is a narrow region that runs along the span which is darker , i.e. where the sublimation rate is higher than elsewhere. This phenomenon which was observed on araldite models in an earlier part of the investigation can now be explained by the existence of a peak in the recovery temperature distribution. Indeed, such sublimation patterns being obtained after a long running time of the tunnel, the model has ample time to reach thermal equilibrium. Furthermore with araldite models the internal heat conduction is not sufficient to smooth out a temperature peak. In the "peak region" , the concentration of chemical increases near the surface and therefore the sublimation rate is accordingly higher.

The existence of a peak in the recovery temperature distribution

followed by fairly low recovery temperatures in transitional reattaching flows on flaps has not been reported yet, as far as the author is aware. This is probably due to the fact that recovery temperatures are not very often measured directly because their measurement requires facilities with long running times. It is often believed that the recovery factor is relatively constant throughout the separated region and approximatively equal to the attached flow value (10, 11, 12). Indirect measurements obtained by extrapolating experimental data to zero heat flux have been made for instance by Larson (13) and Naysmith (14) who did not observe temperature peaks. Seban, Emeny, and Levy (15) who have used a technique similar to the present one , to investigate subsonic turbulent reattaching flows behind a backward facing step, have observed systematically that the recovery factors were substantially below the typical value for turbulent flows of air (0.80 instead of 0.89) which indicated an unbalanced energy distribution in the flow. The authors do not mention the existence of a peak in the recovery temperature distribution although there seems to be a very slight maximum in the figures of their report. In transition studies made with attached flows on hollow cylinders, Brinich (16) reports a peak in recovery factor followed by a drop to the turbulent value , attributed to a violent mixing in the transition region. Brinich also reports (17) peaks and troughs in the recovery factor distributions in turbulent flows near two-dimensional roughness but not in laminar flows.

Recovery Temperatures (Artificial Transition)

Because of the very limited range of Reynolds number available in the present investigation, it was necessary as a view to investigating further types of flows to trigger artificially the transition. This was done by tripping the boundary layer upstream of separation. By selecting a proper size of the roughness and by varying the R_e number in the available range, it was possible to move transition on the 15-deg. flap model from its natural location of x_t = 135 mm at $R_e = 3 \times 10^6$ to x_t = 50 mm, thus

giving various types of transitional reattaching flows, as well as a fully turbulent unseparated flow.

The recovery temperature distributions are shown in figure 8 by smooth curves passing through the experimental points. x_t indicates the location of transition. One can see that the temperature peak moves upstream with transition until the flow becomes attached (i.e. for a unit Reynolds number larger than 2.1×10^6). Then the temperature peaks remain fixed at the nose of the ramp. Following the peak, the temperature drops down to a value which is approximatively the theoritical turbulent flat plate value based on the initial Mach number, i.e. somewhat lower than the one based on the final Mach number which one could expect. Further downstream, the temperature rises very slowly and it seems that a long downstream distance is needed for the boundary layer to readjust itself to a fully turbulent flow.

The temperature peak observed in fully turbulent flow is obviously associated with the rapid pressure rise at the nose of the ramp (see fig. 2g) and no longer with the transition process as it was probably the case in transitional separated flows. This is further demonstrated by the recovery temperature distributions measured in turbulent flows over the various flap models and shown in fig. 9. A temperature peak exists in each case at the nose of the flap, which increases with flap angle. For $\theta = 21°$ the flow separated slightly upstream of the flap and the temperature peak is flatter.

All these results indicate that, when transition is located either downstream or upstream of the reattachment region, the temperature peak is flatter than when transition is located in that region. In the latter case, the temperature peak is possibly due to a combined effect of transition and of a steep pressure rise.

Heat Transfer Measurements

The results of the heat transfer measurements are shown in

in figures 4a to 4f, where the wall temperature T_w in degrees centigrade is plotted versus the streamwise coordinate x in millimetres, for various flap angles, for a stagnation temperature of 27°C (300°K) and for unit Reynolds numbers of I.5 and 3.0×10^6 m^{-1}. These were obtained by dissipating uniformly a certain amount of heat over the whole surface of the models. This amount was not necessarily the same for each flap angle and it was taken into account in reducing the data in the form of $N_u/\sqrt{R_{ex}}$, where the Nusselt number and Reynolds number are based on conditions upstream of the interaction region, i.e. :

$$N_u = \frac{hk_e}{x} \quad ; \quad R_e = \frac{U_e \rho_e x}{\mu_e} \quad ; \quad h = \frac{q}{T_w - T_r}$$

The quantity $N_u/\sqrt{R_{ex}}$, which is theoretically constant and equal to 0.37 for a flat plate with uniform heat flux (5),is plotted versus x in figures 2a to 2h. The heat transfer coefficient h, is inversely proportional to the driving temperature $(T_w - T_{wa})$ which is the difference between the curves given in fig. 4. A summary of the heat transfer results is given in figures 10a and 10b, where smooth curves drawn through the experimental points are shown.

Figures 2 show that the value of $Nu/\sqrt{R_{ex}}$ is constant upstream of the interaction region but lower than theoretically predicted by about 10%. Similar results were previously observed in flat plate studies made by the author (5).

The effect of the ramp is to , first, decrease $N_u/\sqrt{R_{ex}}$ below the flat plate value for all flap angles (even for $\theta = 1.5°$ and $3.0°$ for which the flow was attached to the model surface). $N_u/\sqrt{R_{ex}}$ passes through a minimum and then increases further downstream. This minimum decreases with increasing flap angle until $\theta = 15°$ and then rises again. The lowest value of $N_u/\sqrt{R_{ex}}$ which was measured was of 0.15, i.e. approximatively one third of the plate value.

For unseparated flows, $N_u/\sqrt{R_{ex}}$ increases gradually over the surface of the flap, at a rate which is independent from the unit Reynoid number. For separated flows, the $N_u/\sqrt{R_{ex}}$ begins to increase ahead of the flap, i.e. in the separated flow region where the pressure is constant. The rate of increase over the flap depends upon θ and also strongly on the Reynolds number. A maximum value of $N_u/\sqrt{R_{ex}}$ of 1.8 was measured which is about 5 times the flat plate value. For comparison the heat transfer distribution was measured in the case of fully turbulent flow. The results are shown in fig. 11. There is a steep increase of $N_u/\sqrt{R_{ex}}$ near the nose of the flap, followed by a rather constant value. These constant values are also shown in fig. 10b for comparison with the laminar and transitional results. Similar values were obtained in turbulent flow by Sayano, Bausch and Donnelly at Douglas Cy (10).

As already mentioned, for $\theta < 5°$ the effect of R_e on the curve $N_u/\sqrt{R_{ex}}$ versus x is small. For $\theta = 10°$, the Reynolds number has a large effect on the heat transfer rise over the flap and no influence on the heat transfer near separation and in the separated region of the flow. For $\theta > 10°$, the effect of R_e is felt over the entire interaction region. The influence of the location of transition is obviously important.

No rise in heat transfer was observed at separation like Miller et al found (19), which was attributed to a separation vortex. No peak in heat transfer was measured in the reattachment region as is typically observed in cavity flows; see for instance Nicoll's results at hypersonic speed (20).

CONCLUSIONS

Laminar and transitional reattaching flows were obtained in the range of unit Reynolds number of 1.5 to 3.0×10^6 per metre and flap angles up to 21° at a Mach number of 2.02. It was necessary to trip the boundary layer to obtain fully turbulent flows.

A nearly constant pressure developed in the separated region of

the flow for flap angles equal or larger than 7 degrees. In these cases, transition was in the reattachment zone. Plateau pressures were in agreement with Chapman's formulae for laminar flows. The pressure distribution is rather sensitive to the location of transition. For turbulent flows, flap angles of about 21° are needed to separate the boundary layer.

A marked peak of recovery temperature exists near reattachment for transitional flows, followed by substantially low temperatures downstream of reattachment. This peak increases, while the downstream temperature decreases when the unit Reynolds or the flap angle are increased. Transition seems to be located in the temperature-peak region. However, the existence of the peak can also be caused by the large pressure rise at reattachment, as shown by the unseparated turbulent flow results. Long downstream distances are necessary for the boundary layer to readjust itself to a fully turbulent flow.

Heat transfer distributions are even more sensitive to the location of transition than the pressure distributions. The effect of the flap is generally, to first lower the heat transfer to a minimum, which can reach in certain cases one third of the flat plate value, and then to increase it at a rate which increases with Reynolds number and flap angle. Heat transfer results are generally in agreement with measurements made by other investigators with isothermal models.

PART II

INTRODUCTION

There has been considerable interest in the use of separated flows as a means of reducing the aerodynamic heating of high speed vehicles, since Chapman (18) published in 1956 a theoretical investigation which showed that for the laminar separated flow model he chose, the average heat transfer rate was only 56 % of that which would occur with an attached flow. These predictions were confirmed for cavity flows by Larson (13) at supersonic speeds and by Nicoll (20) in the Princeton University Helium hypersonic tunnel. However, it was observed that separated flow produced other less desirable effects, inasmuch as local heat transfer coefficients several times larger than the attached flow value existed in the vicinity of reattachment. As a result, the laminar cavity flow offered no net advantage.

Chapman (18) also showed that a small amount of fluid injected into the separated region could reduce the wall heat transfer rate to zero. It was therefore important to verify experimentally if one could improve the rather discouraging results obtained in the absence of mass injection. It was thus decided to carry on an experimental investigation in this direction at the von Karman Institute for Fluid Dynamics at supersonic and hypersonic speeds.

Difficulties were met initially in obtaining sizable regions of laminar separated flow with mass injection at supersonic speeds and also in designing a model using a steady state technique of heat transfer measurements. Therefore the investigation was later mainly oriented towards the low hypersonic range (M of about 7). This was further motivated by the encouraging results obtained in an exploratory investigation made by Nicoll (21) at M = 11 to 12 in a Helium wind tunnel, which became available to the author in the course of this program.

This part of the research has been sponsored by the Air Force Office of Scientific Research, O.A.R., through the European Office, Aerospace Research, United States Air Force, under Grant AF EOAR 66-6.

EQUIPMENT AND MODELS

Wind tunnel

The tests were conducted in the VKI 12 cm x 12 cm blow down hypersonic wind tunnel H-1 at a Mach number of 6.7, at stagnation pressures of 30 to 32 atmospheres absolute and at stagnation temperatures of 350 to 400°C. The free stream Reynolds numbers based on a length of one inch was of about 5×10^5.

Tunnel H-1 has a running time of two minutes. It was equipped with a two-dimensional nozzle with adjustable throat giving a Mach number of 6.7 at the nose of the model and 7.0 at its base.

Flow pictures were taken with shadow and single pass schlieren systems and a spark light source of a few micro-seconds duration time.

Heat transfer measurements

Heat transfer rates were measured with a thin skin transient technique. Early measurements were made by injecting the model into the test section after starting the tunnel. Later, models were fixed in the test section and the tunnel was started with a quick acting valve. In both cases, it was estimated that the flow was established after a few hundredths of a second.

Temperature-time histories were measured on a CEC galvanometric recorder - type 5-124, equipped with 1.46 and 1.75 millivolts/inch galvanometers. Temperature derivatives $\frac{\partial T}{\partial t}$ were measured a fraction of a second after the starting time of the tunnel, while the model was still at uniform (i.e. room) temperature. The heat flux per unit time and unit area was calculated from

$$q = \rho c d \frac{\partial T}{\partial t} .$$

The density (ρ) and specific heat (c) of the stainless steel model skin were given by the manufacturer. The skin thickness (d) used in the data presented in this report has been estimated with thickness gages,

except for the cone model. Accurate measurements of the thickness distribution of the skin necessitates the destruction of the models which has not been attempted at this stage of the investigation, except for the cone model.

Also, no correction was made to include the effect of transverse heat conduction through the model skin due to the limited number of thermocouples that were used in these preliminary tests.

The recovery temperature was assumed constant and equal to the cone value. This assumption is justified by the results obtained by Nicoll at hypersonic speeds.

Models and injection system

The main dimensions in millimetres, the location of the thermocouples and the inside arrangement of the final heat transfer model are shown in figure 12. The model consisted of a cone, with 10° half apex angle, into which an annular cavity was made. It was hollow and machined from stainless steel. The thickness of its skin was of 0.8 mm. The cavity was 10 mm wide at its bottom and 4 mm deep. The reattachment side was, in the meridian plane, formed by a circular arc with a 4 mm radius. The annular slot was 1 mm wide.

Copper and constantan wires of 0.06 mm and 1 mm in diameter respectively were used for the thermocouples. They were inserted into small holes drilled through the model skin and silver soldered.

Atmospheric air was used in the injection system. The flow rate, determined by a calibrated diaphragm, was varied between zero and the boundary layer mass flow at separation (Q_{BL}). The latter was computed from the flat plate theory of Chapman and Rubesin based on conditions along the cone and divided by $\sqrt{3}$. In the present tests Q_{BL} was equal to 18 litres/minute (under standard atmospheric conditions).

RESULTS AND DISCUSSION

Preliminary tests were made, using various cone angles and different sizes and locations of the cavity, to determine the final configuration shown in figure 12. The width of the cavity was selected equal to 14 mm to maintain steady flow and the reattachment side (i.e. the downstream top corner of the cavity) was rounded off to allow more detailed heat transfer measurements at reattachment. Shadowgraphs showed that the flow was fully laminar in the absence of injection. With injection, transition moved upstream. For an injection rate $c_q = 0.25$, it was 4 to 5 cavity widths downstream of reattachment and for $c_q = 1.0$, only one cavity width downstream ; c_q being the ratio of the injected mass flow to the boundary layer mass flow at separation. Shadowgraphs also showed that a shock wave existed at reattachment in the case of no injection, which disappeared at an injection rate lower than 0.25.

To check the accuracy of the thin skin technique of heat transfer measurements, tests were first made with a simple cone model for which an exact laminar theory was available. Experimental results determined within $\pm$ 2% were found to be 5 to 10 % lower than the theoretical values. Such a difference could be attributed either to an incorrect value of the product ρc or to thermocouple effects or, also, to a slight incidence of the cone and non-uniformities of the flow in the test section. However, it was believed that this agreement was sufficiently good so as to be able to apply the same technique to the cone-cavity model.

The results of heat transfer measurements on the cone-cavity model are plotted in figures 13 and 14, where x is the coordinate along the cone surface as indicated in figure 12 ; q_c is the heat flux at the surface of a conical model having the same apex angle as the cone-cavity model ; q_o is the heat flux on the cone-cavity model without mass injection and q the corresponding heat flux with mass injection. c_q is the mass injection rate, i.e. the ratio of the injected mass flow to the mass flow in the boundary layer at separation.

Curve (a) in figure 13 shows the effect of the cavity (i. e. of flow separation) on the heat transfer distribution in the absence of mass injection. The data point indicated at each thermocouple location gives the mean arithmetic value of q_o/q_c computed from a large number of tests. A smooth curve is shown in the figure passing through these points. It is seen that, although the heat transfer rate is considerably reduced at the cavity floor, the existence of a large peak at reattachment (more than twice the attached flow value) reduced the net advantage of flow separation.

The other curves, shown in figure 13, compare the heat transfer distributions with and without mass addition. The scatter of the results is shown by the vertical bars. It is seen that mass injection reduced the heat transfer rates over the whole surface of the model for values of c_q up to 0.25. This is particularly so in the cavity region and at reattachment. For c_q larger than 0.25, the heat transfer rate increases very much over the downstream portion of the model. This is attributed to the upstream displacement of transition.

The same results are plotted in a different way in figure 14, where the heat flux q is referred to the attached flow or cone value q_c. It is seen that the heat transfer peak at reattachment decreases as mass is injected into the cavity. For $c_q = 0.10$, the peak still exists although q/q_c has become smaller than one. For values of c_q in the range 0.10 to 0.25, the peak has disappeared while, as mentioned previously, the reattachment shock has vanished and the ratio q/q_c is less than unity over the whole surface of the model. At $c_q = 0.25$, the heat transfer to the cavity floor is extremely small. According to Chapman's theory (18), this heat transfer should be zero at $c_q = 0.26$, which is thus in very good agreement with the present experimental results. For c_q larger than 0.25, the heat transfer rate increases considerably above the cone value, as a result of the upstream displacement of transition.

The results of this investigation agree very well with Nicoll's results obtained at M = 11.5 in a helium wind tunnel.

CONCLUSIONS

Cone-cavity models have been designed and tested that produced steady laminar flow with mass injection into the cavity.

The heat transfer, although greatly reduced at the floor of the cavity, increased considerably at reattachment so that the laminar cavity flow offers no net advantage.

A small amount of mass injection had a pronounced effect on the heat transfer rate at reattachment, inasmuch as it suppressed the heat transfer peak. There is an optimum value of the injection rate, namely one quarter of the boundary layer mass flow at separation, at which the heat transfer is almost zero in the cavity and stays below the cone value over the whole surface of the body.

REFERENCES

1. GINOUX, J.J. - The existence of three-dimensional perturbations in the reattachment of a two-dimensional supersonic boundary layer after separation. Agard Report 272, 1960
2. GINOUX, J.J. - Leading edge effect on separated supersonic flows. Proceedings of ICAS III. Stockholm 1962
3. GINOUX, J.J. - Streamwise vortices in Laminar Reattaching Flows. Recent developments in Boundary Layer Research. AGARDograph 97, Part I. Naples, May 1965
4. GINOUX, J.J. - Laminar Separation in Supersonic and Hypersonic Flows. Grant AF EOAR 65-11. Final Report October 1965
5. GINOUX, J.J. - A Steady State Tecnique for local heat-transfer measurement and its application to the flat plate. - J. of Fluid Mechanics, Vol. 19, part 1, pp 21-29, 1964
6. LEES, L. and REEVES, B.L. - Supersonic Separated and reattaching laminar flows. General theory and application to adiabatic boundary layer. Shock wave interactions. Galcit Techn. Rep. n°3, oct. 1963.
7. NIELSEN, J.N., LYNES, L.L. and GOODWIN, F.K. - Calculation of laminar separation with free interaction by the method of integral relations. Tech. Rep. AFFDL-TR-65-107 October 1965
8. HAKKINEN, R.J., GREBER, I., TRILLING, L., ABARBANEL, S.S. - The interaction of an oblique shockwave with a laminar boundary layer. NASA TM Memo 2-18-59W. March1959
9. CHAPMAN, D.R., KUEHN, D.M., and LARSON, H.K. - Investigation of separated flows in supersonic and subsonic streams with emphasis on the effect of transition- NACA TN 3869, 1957.
10. WUERER, J.E. and CLAYTON, F.I. - Flow Separation in high speed flight. Areview of the state-of-the-art. Douglas Report S.M. - 46429 - April 1965.

11. ROM, J. and SEGINER, A. - Laminar heat transfer to a two-dimensional backward facing step from the high enthalpy supersonic flow in the shock tube. AIAA Journal - Vol 2 - n°2 - Feb. 64

12. BECKER, J. V. and KORYCINSKI, P. F. - Heat transfer and pressure distribution at M=6.8 on bodies with conical flares and extensive flow separation- NASA TN D - 1260 - April 1962

13. LARSON, H. K. - Heat transfer in separated flows -JAS Vol 26, p731, Nov 59

14. NAYSMITH, A. - Heat transfer and boundary layer measurements in a region of supersonic flow separation and reattachment RAE , TN AERO 2558 - May 1958

15. SEBAN, R. A. , EMERY, A. and LEVY, A. - Heat transfer to separated and reattached subsonic turbulent flows obtained downstream of a surface step - JAS - December 1959

16. BRINICH, P. F. - A study of boundary layer transition and surface temperature distributions at M=3.12 - NACA , TN 3509 July 1955

17. BRINICH, P. F. - Recovery temperatures and heat transfer near two dimensional roughness elements at M=3.1 NACA TN 4213 - Feb. 1958

18. CHAPMAN, D. R. - A theoritical analysis of heat transfer in regions of separated flow. NACA TN 3792 (1956)

19. MILLER, D. S. , HYMAN, R. and CHILDS, M. E. - Mach 8 to 22 studies of flow separations due to deflected control surfaces. AIAA Journal , Vol 2 , n°2 , Feb. 1964

20. NICOLL, K. M. - A study of laminar hypersonic cavity flows. AIAA Journal - Vol 2, n°3 - 1535 - 1541 - September 1964.

21. NICOLL, K. M. - Mass injection in a hypersonic cavity flow. ARL 65-90 - May 1965.

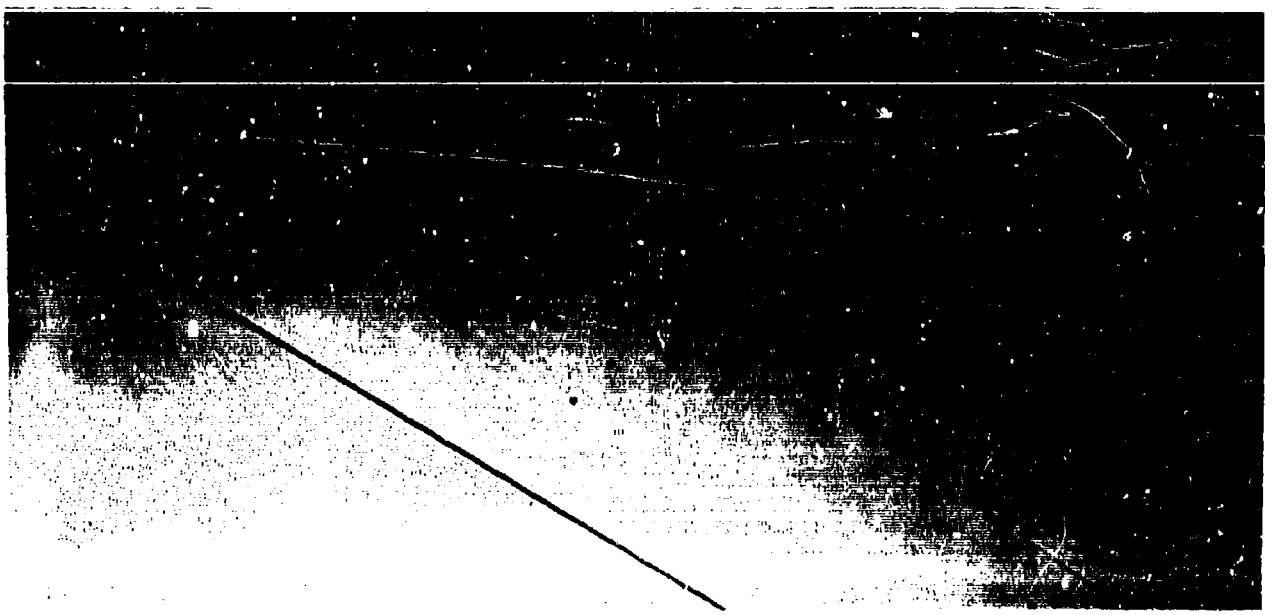

a) $R_e = 1.5 \times 10^6\ m^{-1}$

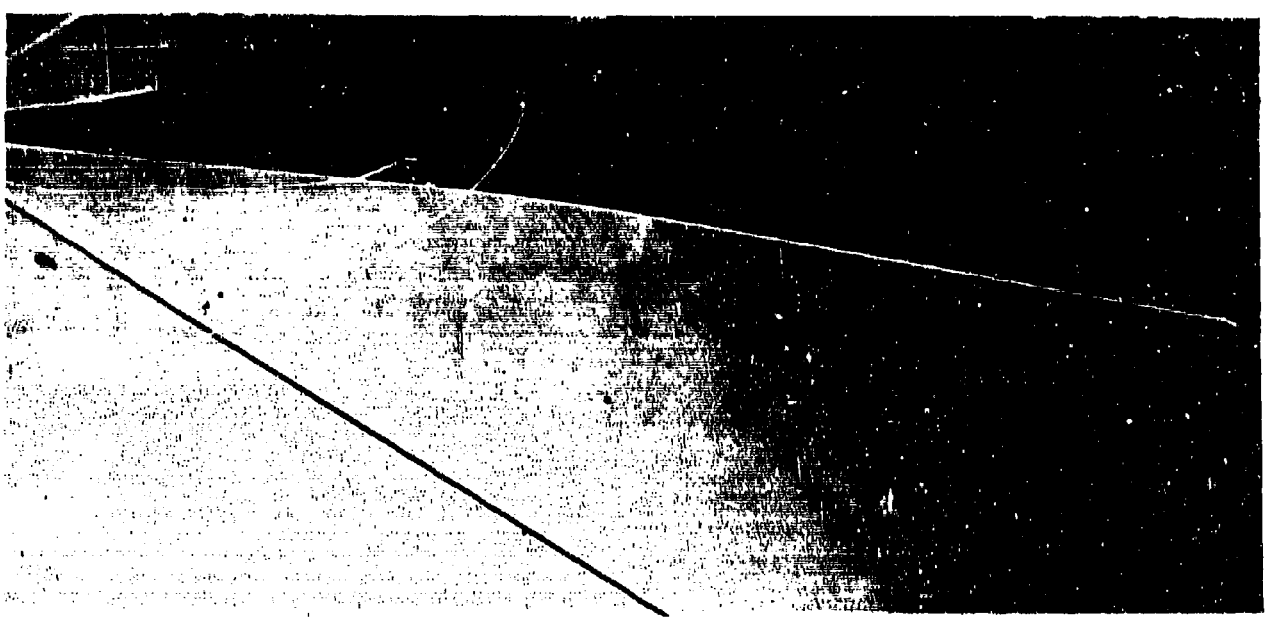

b) $R = 2.2 \times 10^6\ m^{-1}$

Fig.1 - SHADOWGRAPHS OF THE FLOW AROUND A 5 deg. FLAP

c) $R_e = 1.5 \times 10^6\ m^{-1}$

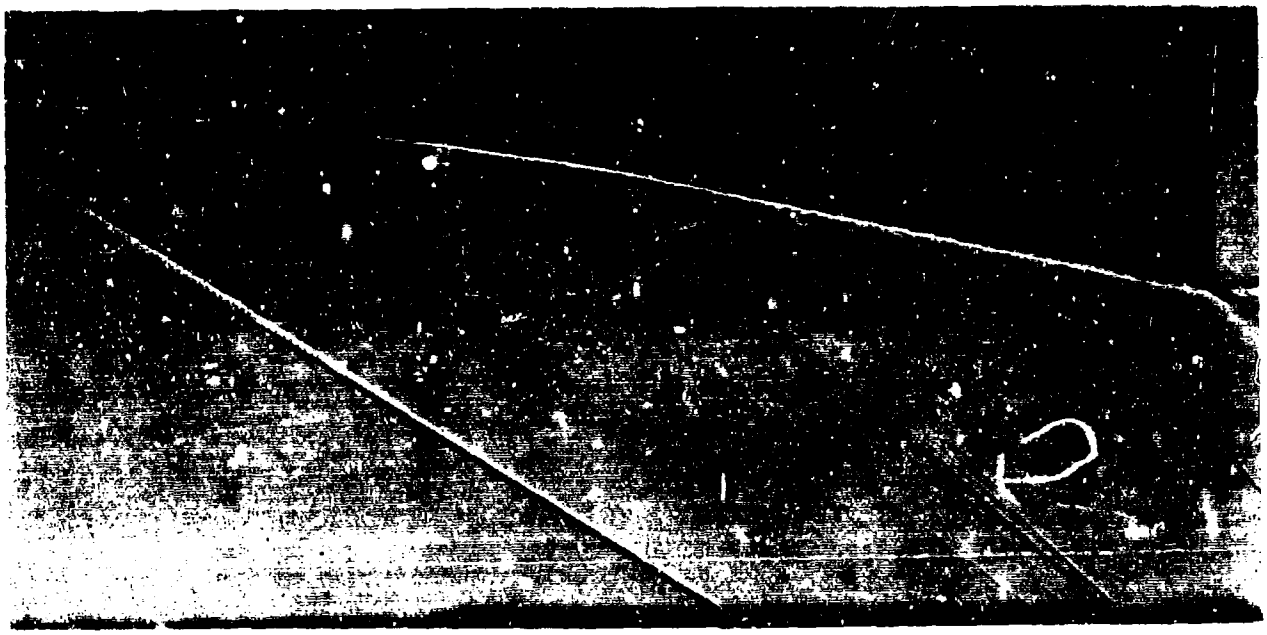

d) $R_e = 3.0 \times 10^6\ m^{-1}$

Fig.1- SHADOWGRAPHS OF THE FLOW AROUND A 7 deg. FLAP.

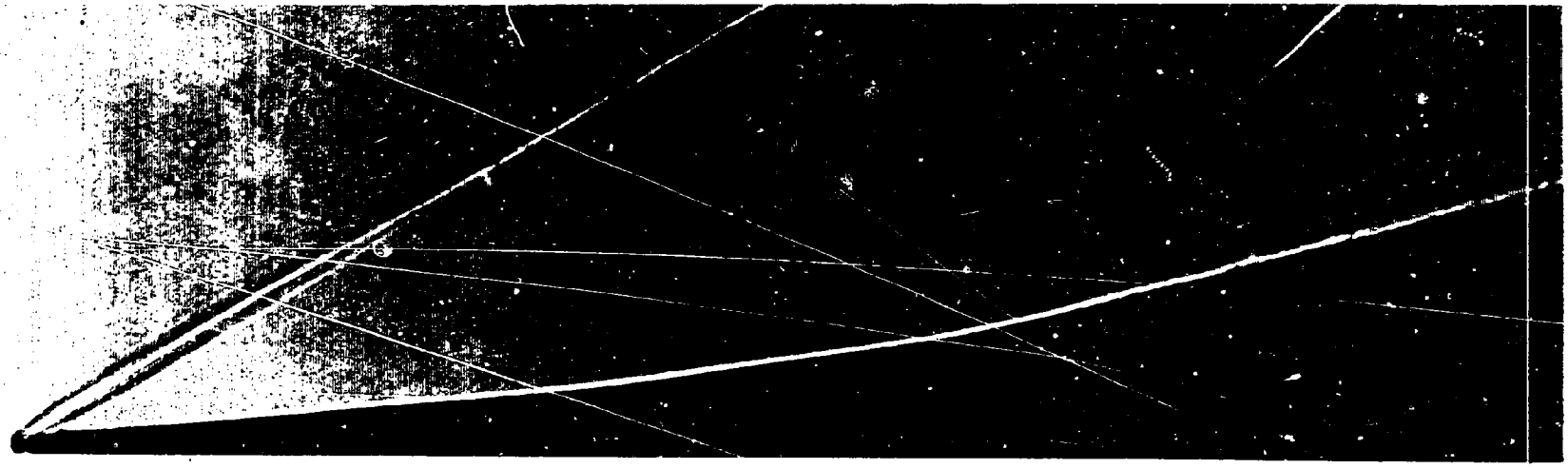

e) $R_e = 1.5 \times 10^6\ m^{-1}$

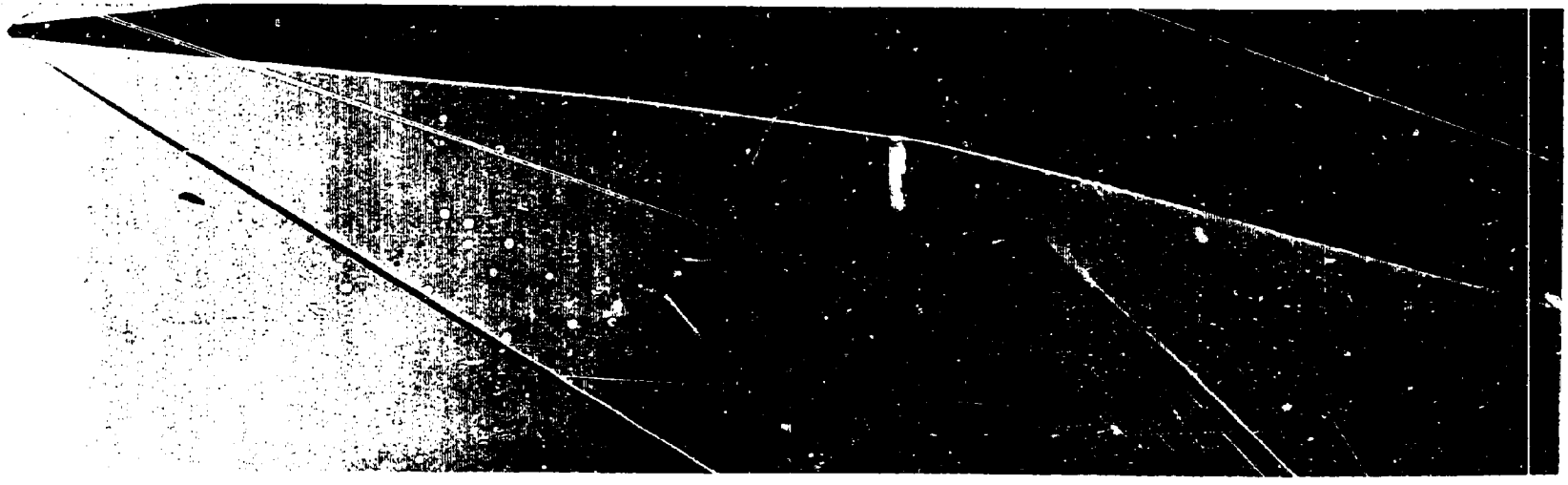

f) $R_e = 3.0 \times 10^6\ m^{-1}$

Fig.1 - SHADOWGRAPHS OF THE FLOW AROUND A 10 deg. FLAP

g) $R_e = 1.0 \times 10^6\ m^{-1}$

h) $R_e = 1.5 \times 10^6\ m^{-1}$

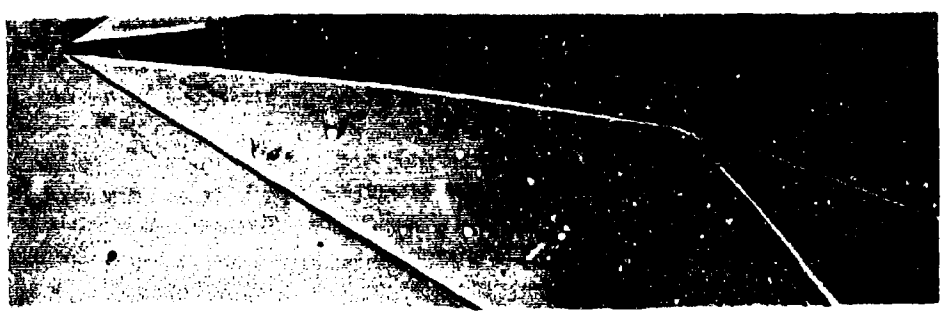

i) $R_e = 3.0 \times 10^6\ m^{-1}$

Fig. 1 - SHADOWGRAPHS OF THE FLOW AROUND A 15 deg. FLAP

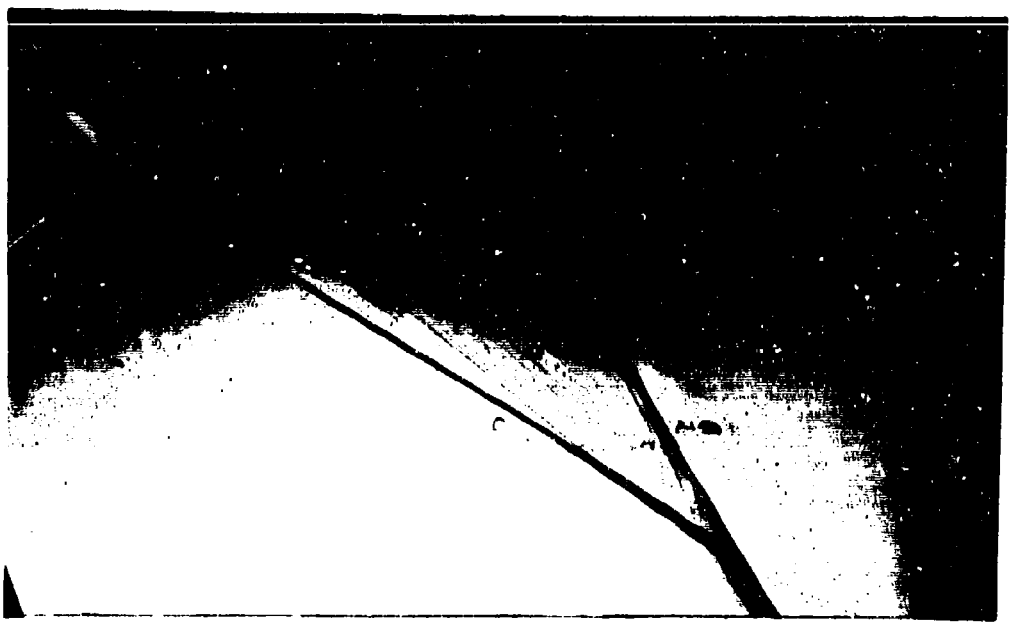

j) $R_e = 1.5 \times 10^6\ m^{-1}$

k) $R_e = 3.0 \times 10^6\ m^{-1}$

Fig.1 - SCHLIEREN PHOTOGRAPHS OF THE FLOW AROUND A 21 deg. FLAP.

$R_e = 3.0 \times 10^6\ m^{-1}$

Fig. 11 - SCHLIEREN PHOTOGRAPH OF THE TURBULENT FLOW OVER A 10 deg. FLAP

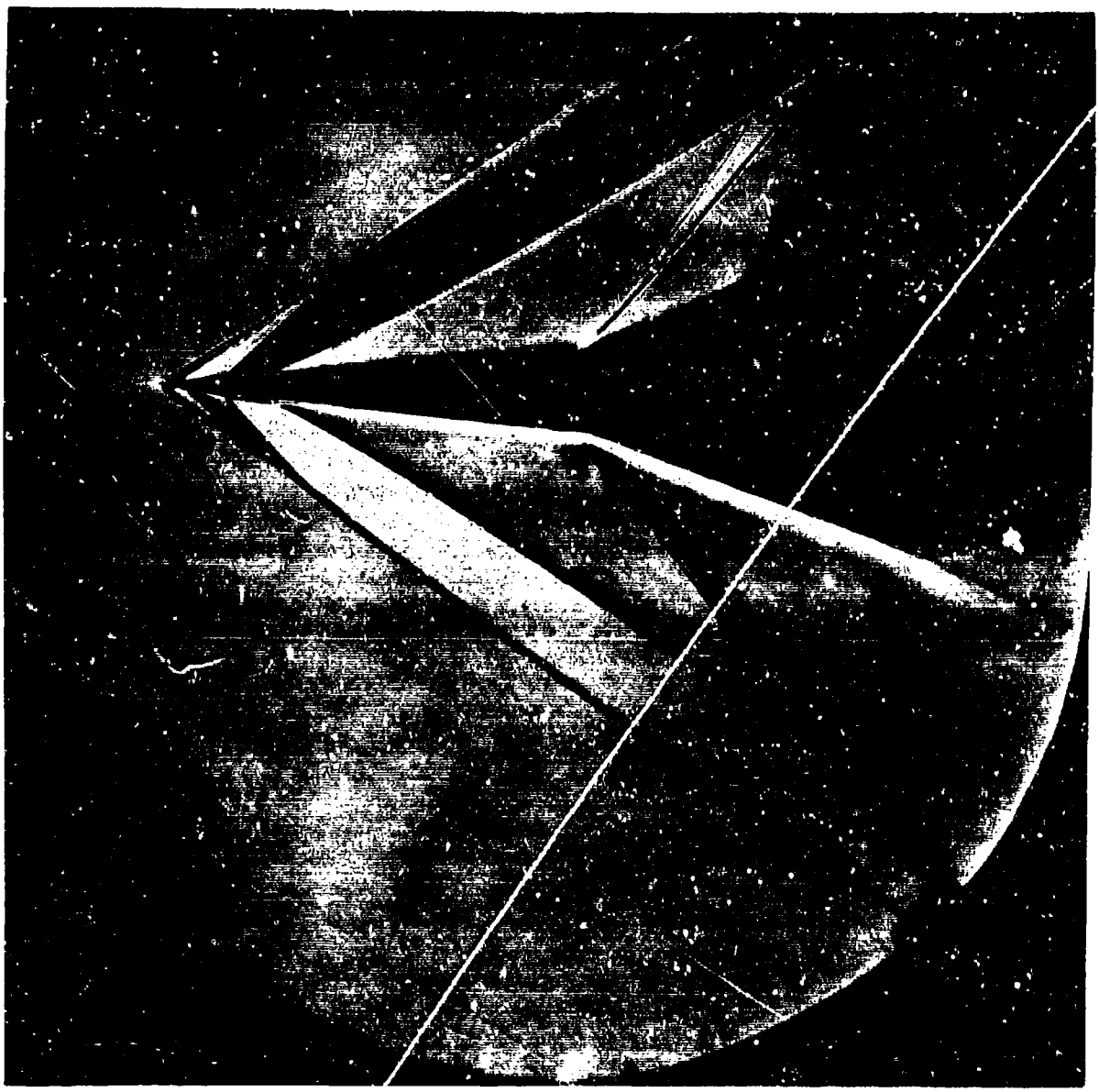

$R_e = 3.0 \times 10^6\ m^{-1}$

Fig.1m - SCHLIEREN PHOTOGRAPH OF THE TURBULENT FLOW OVER A 15 deg. FLAP

$R_e = 3.0 \times 10^6\ m^{-1}$

Fig. 1n - SCHLIEREN PHOTOGRAPH OF THE TURBULENT FLOW OVER A 21 deg. FLAP

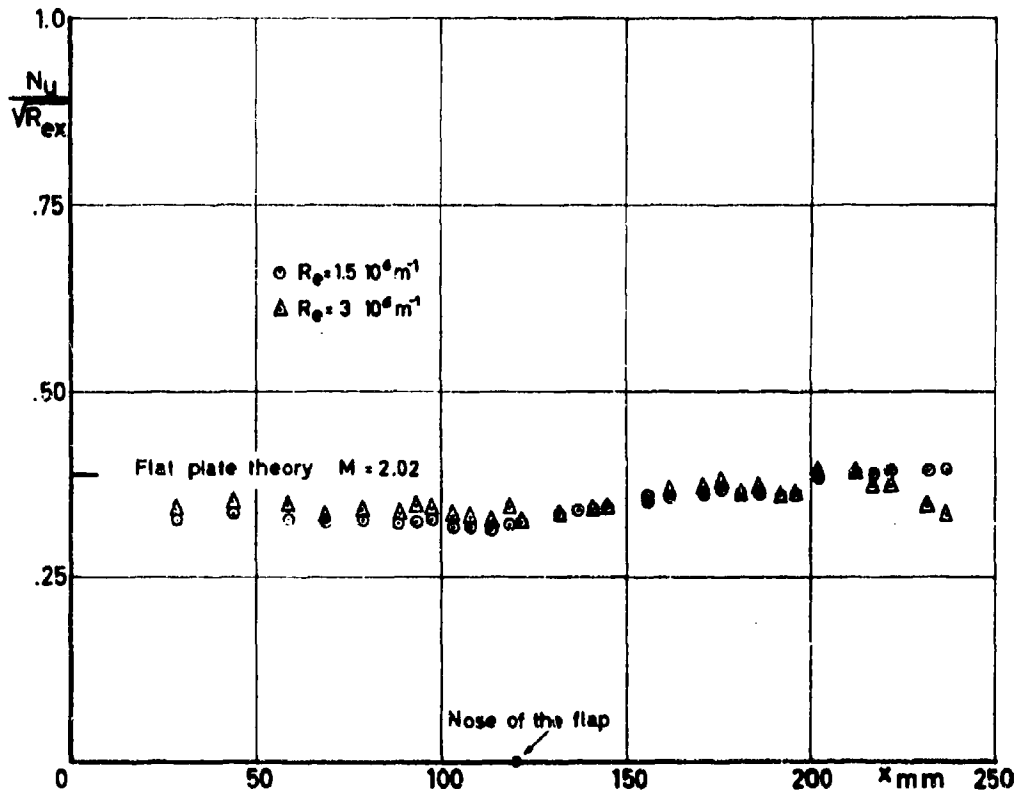

Fig. 2a – HEAT TRANSFER DISTRIBUTION OVER A 1.5° FLAP (Model CCA-4)

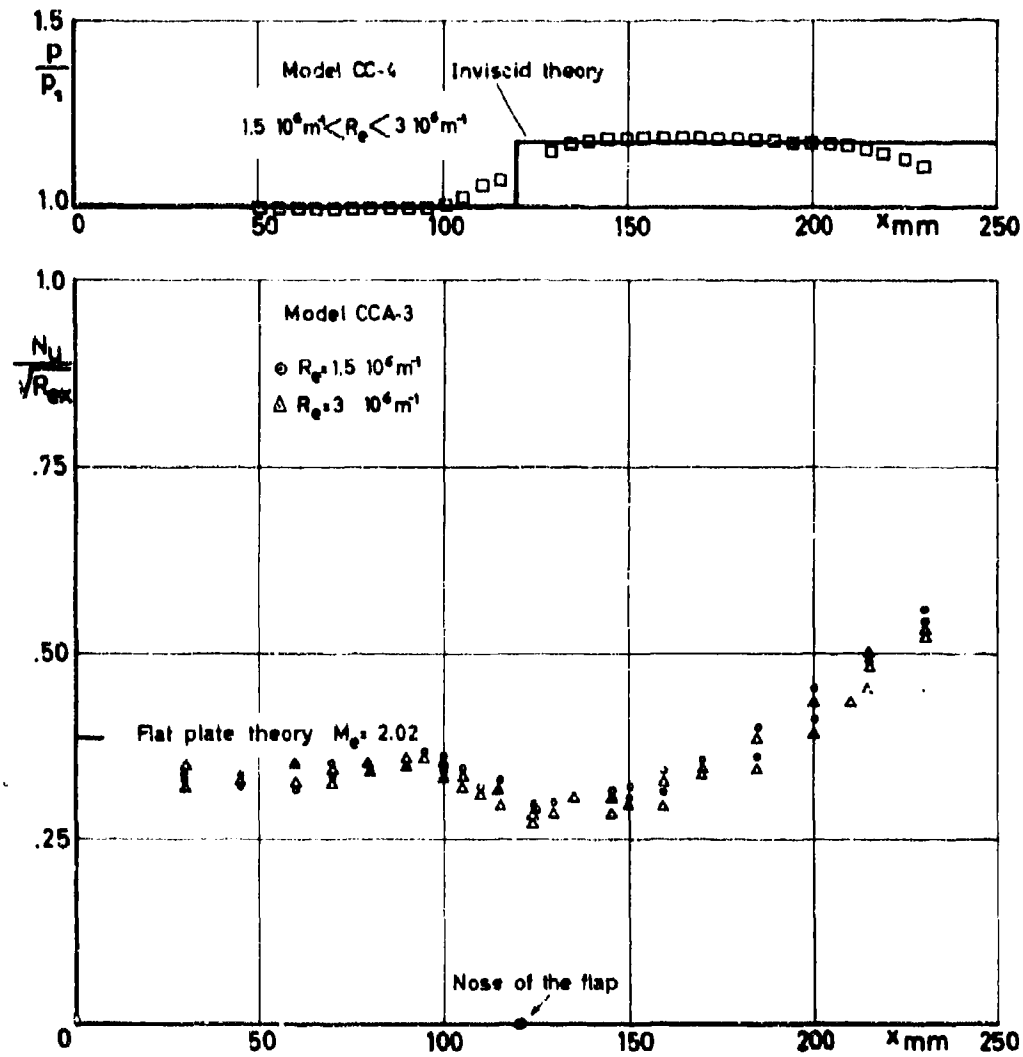

Fig. 2b.- PRESSURE AND HEAT TRANSFER DISTRIBUTIONS OVER A 3° FLAP
Models CC-4 and CCA-3

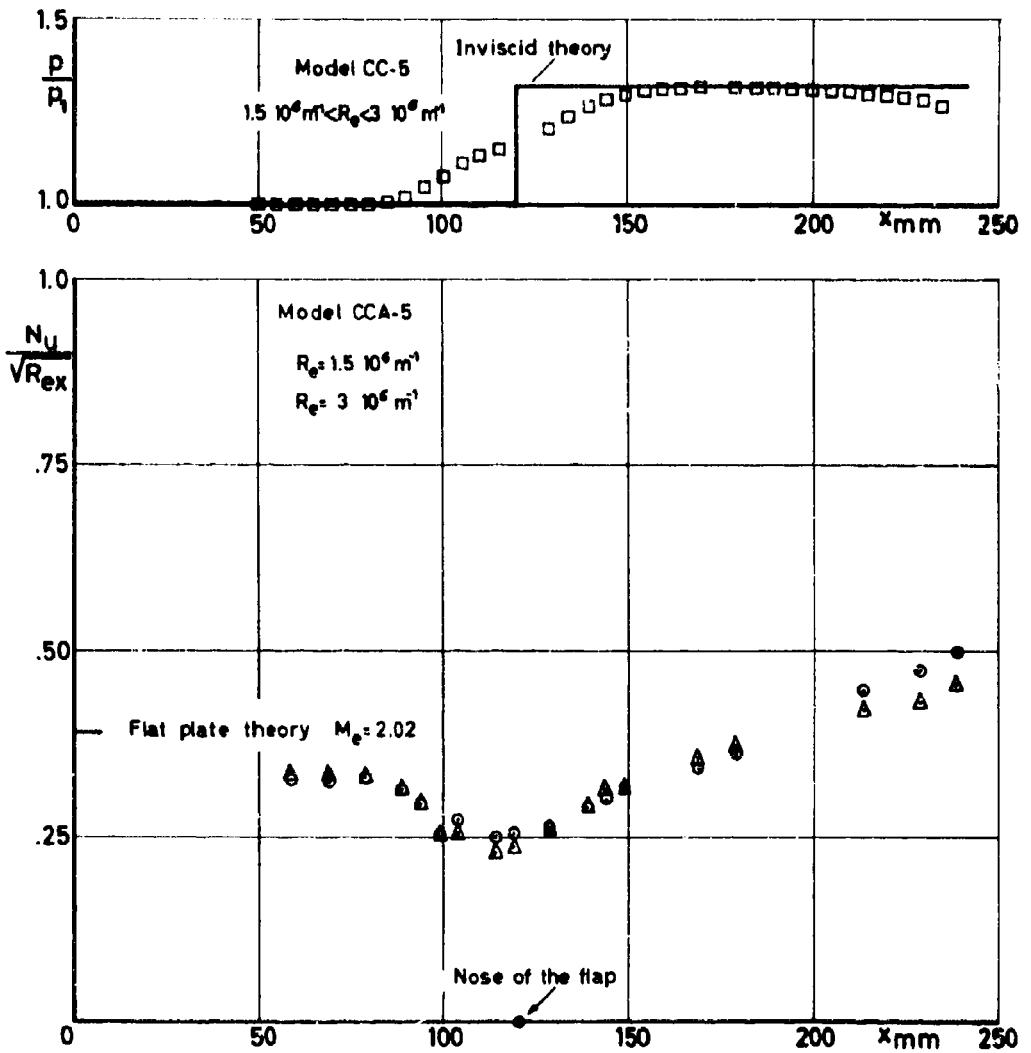

Fig.2c-PRESSURE AND HEAT TRANSFER DISTRIBUTIONS OVER A 5° FLAP
Models CC-5 and CCA-5

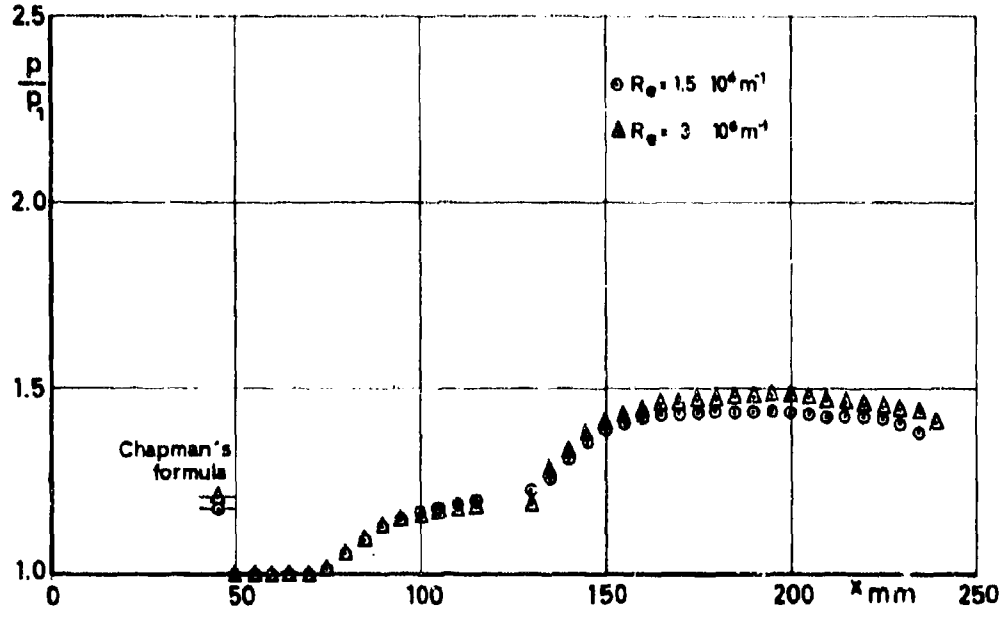

Fig. 2 d - STATIC PRESSURE DISTRIBUTIONS OVER A 7° FLAP (Model CC-7)

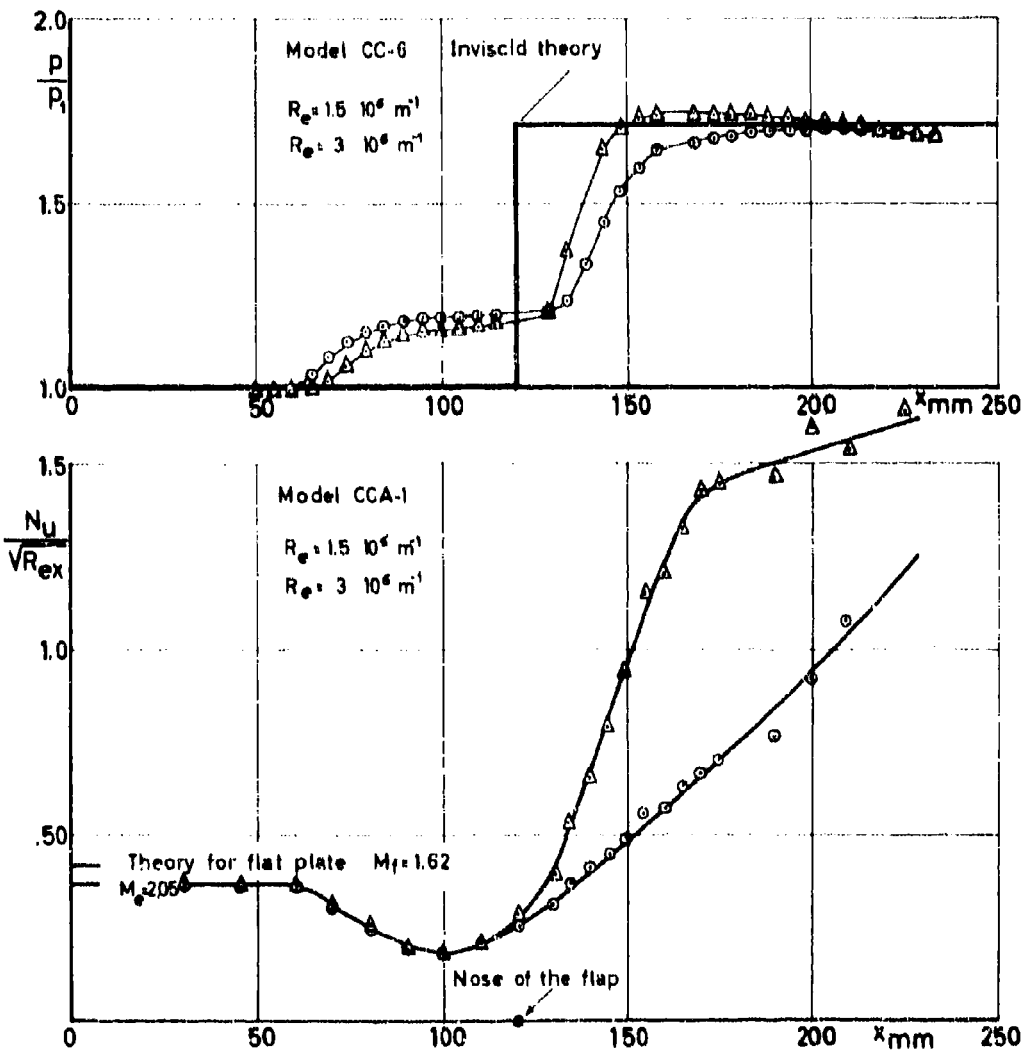

Fig.2 e-PRESSURE AND HEAT TRANSFER DISTRIBUTIONS OVER A 15° FLAP
Models CC-6 and CCA-1

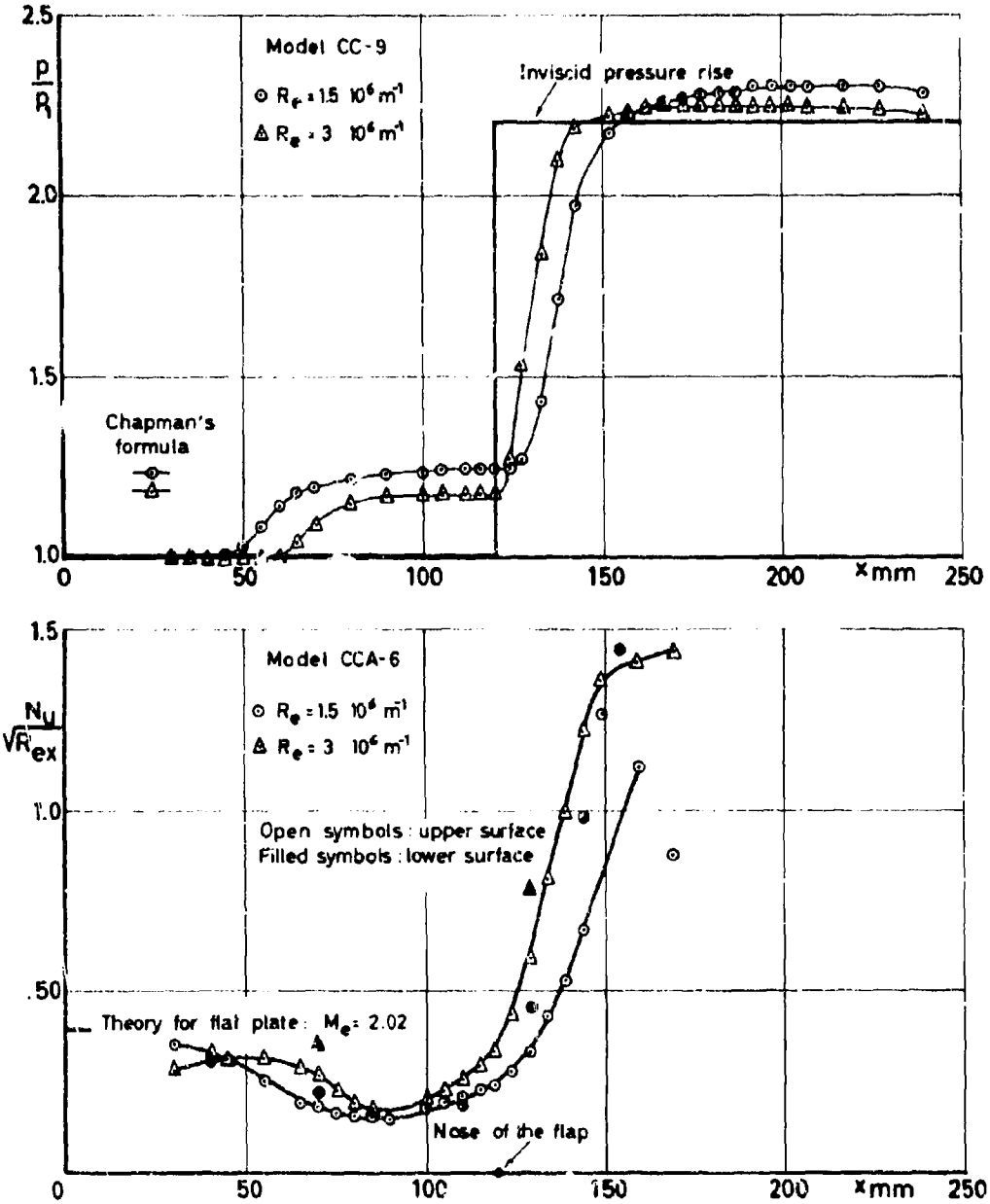

Fig.2 f - PRESSURE AND HEAT TRANSFER DISTRIBUTIONS OVER A 15° FLAP
Models CC-9 and CCA-6.

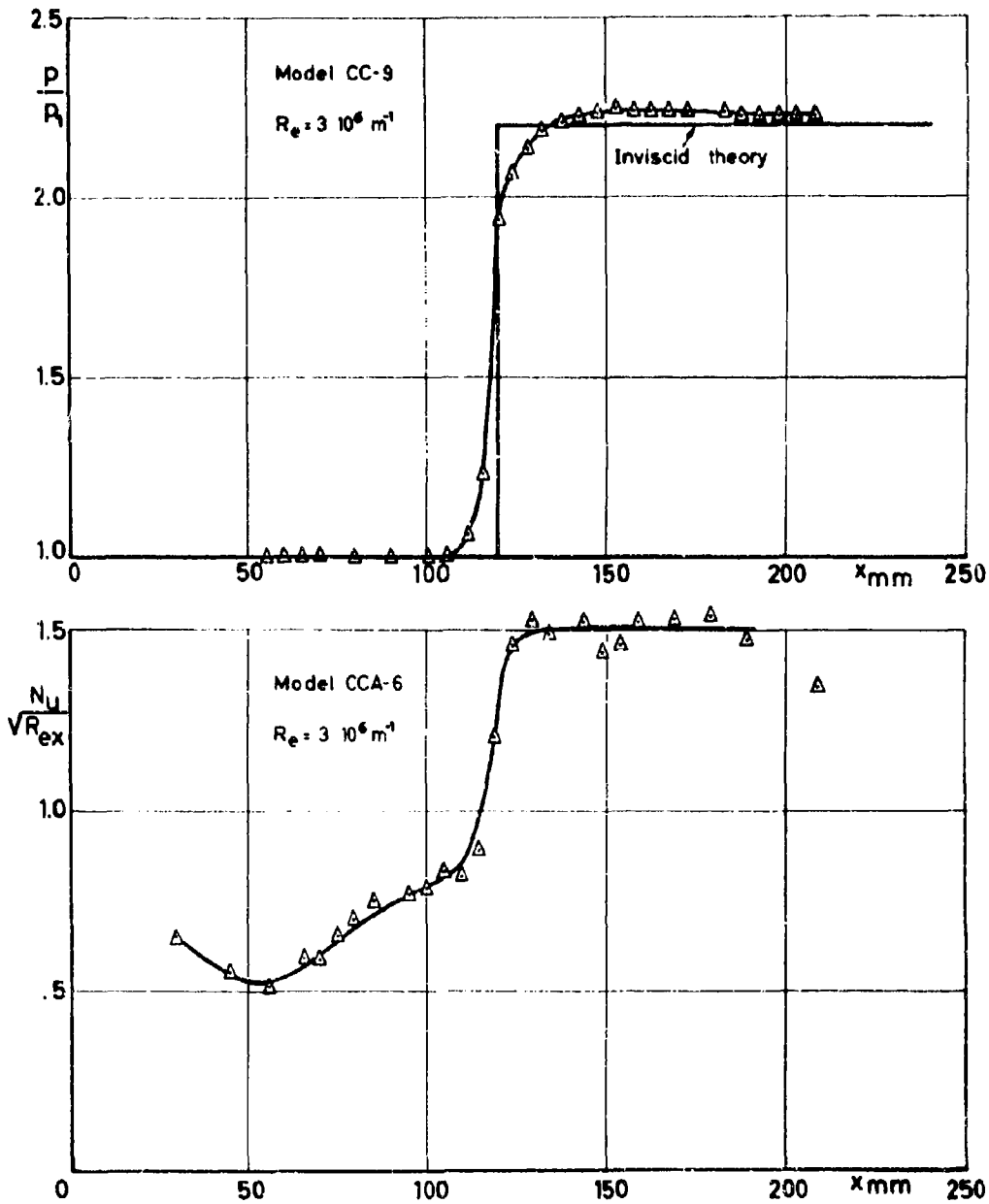

Fig. 2g - PRESSURE AND HEAT TRANSFER DISTRIBUTIONS OVER A 15° FLAP TURBULENT FLOW - Models CC-9 and CCA-6.

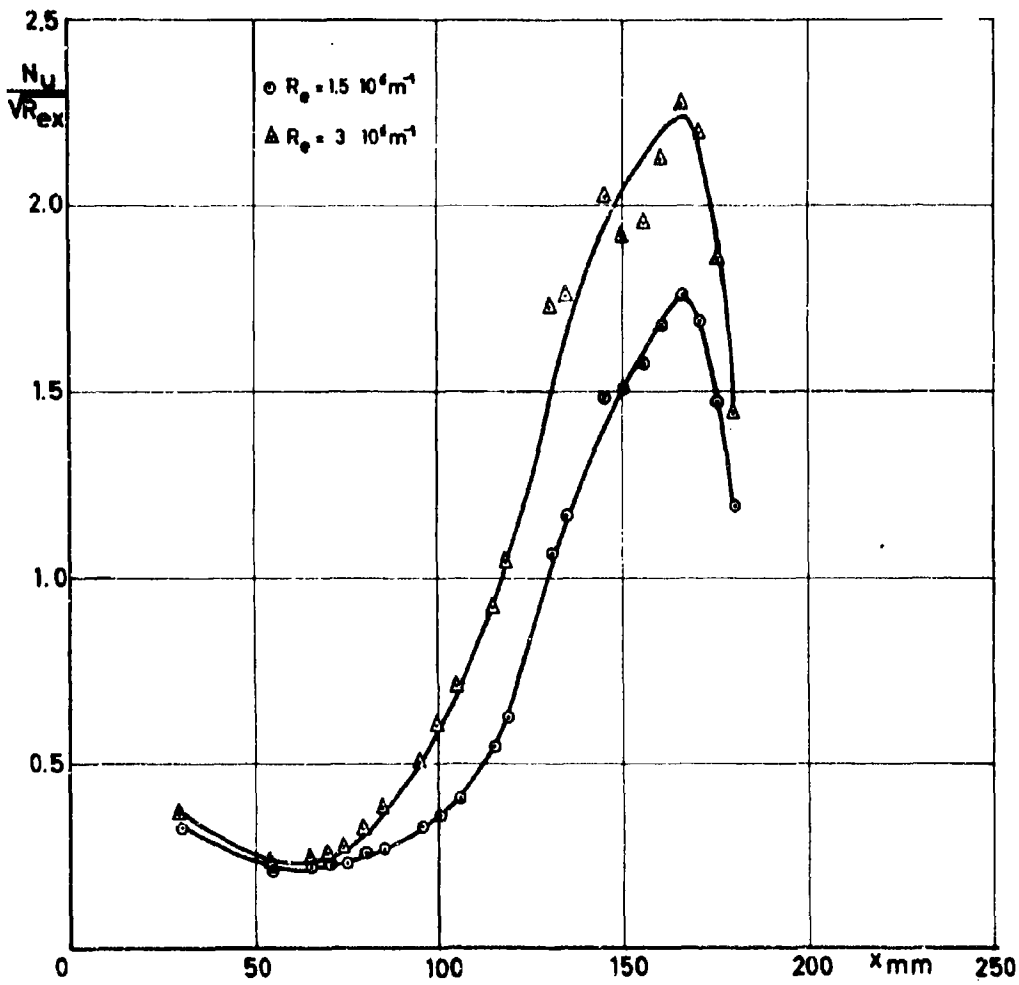

Fig. 2h - HEAT TRANSFER DISTRIBUTION OVER A 21° FLAP (Model CCA-7)

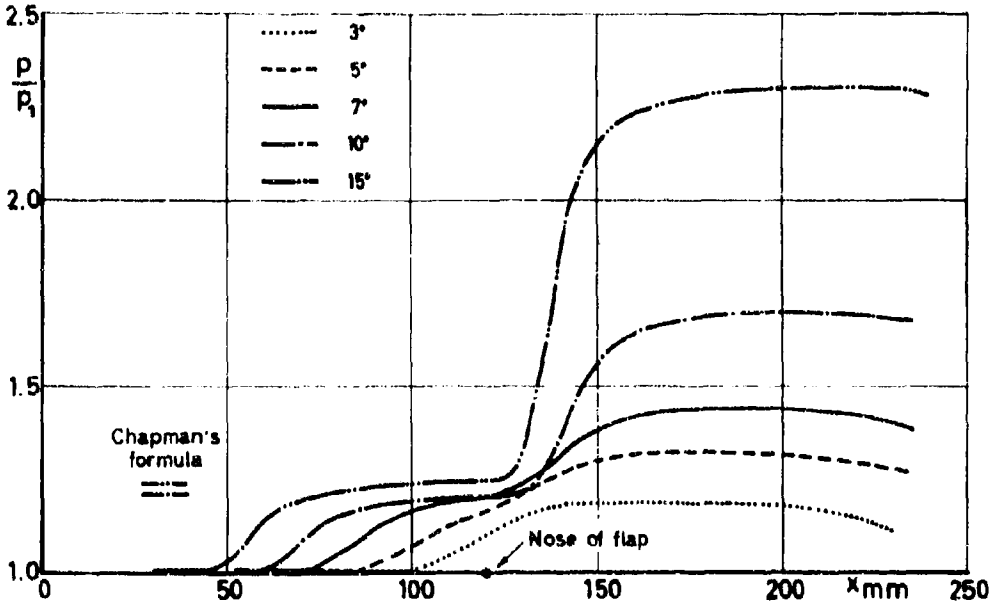

Fig.3a - SUMMARY OF THE STATIC PRESSURE DISTRIBUTIONS FOR VARIOUS FLAP ANGLES - $R_e = 1.5\ 10^6\ m^{-1}$

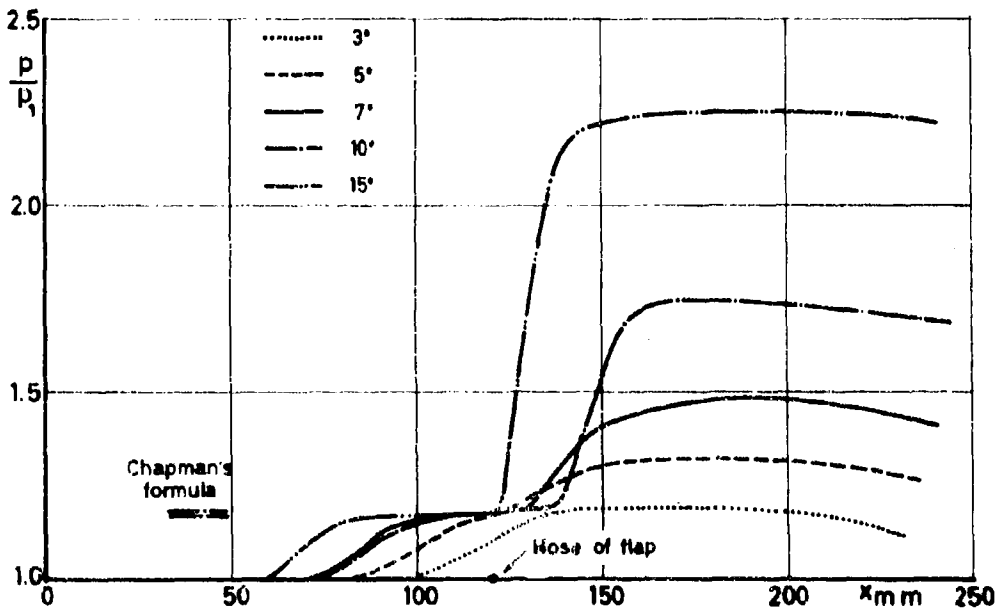

Fig.3b - SUMMARY OF THE STATIC PRESSURE DISTRIBUTIONS FOR VARIOUS FLAP ANGLES - $R_e = 3\ 10^6\ m^{-1}$

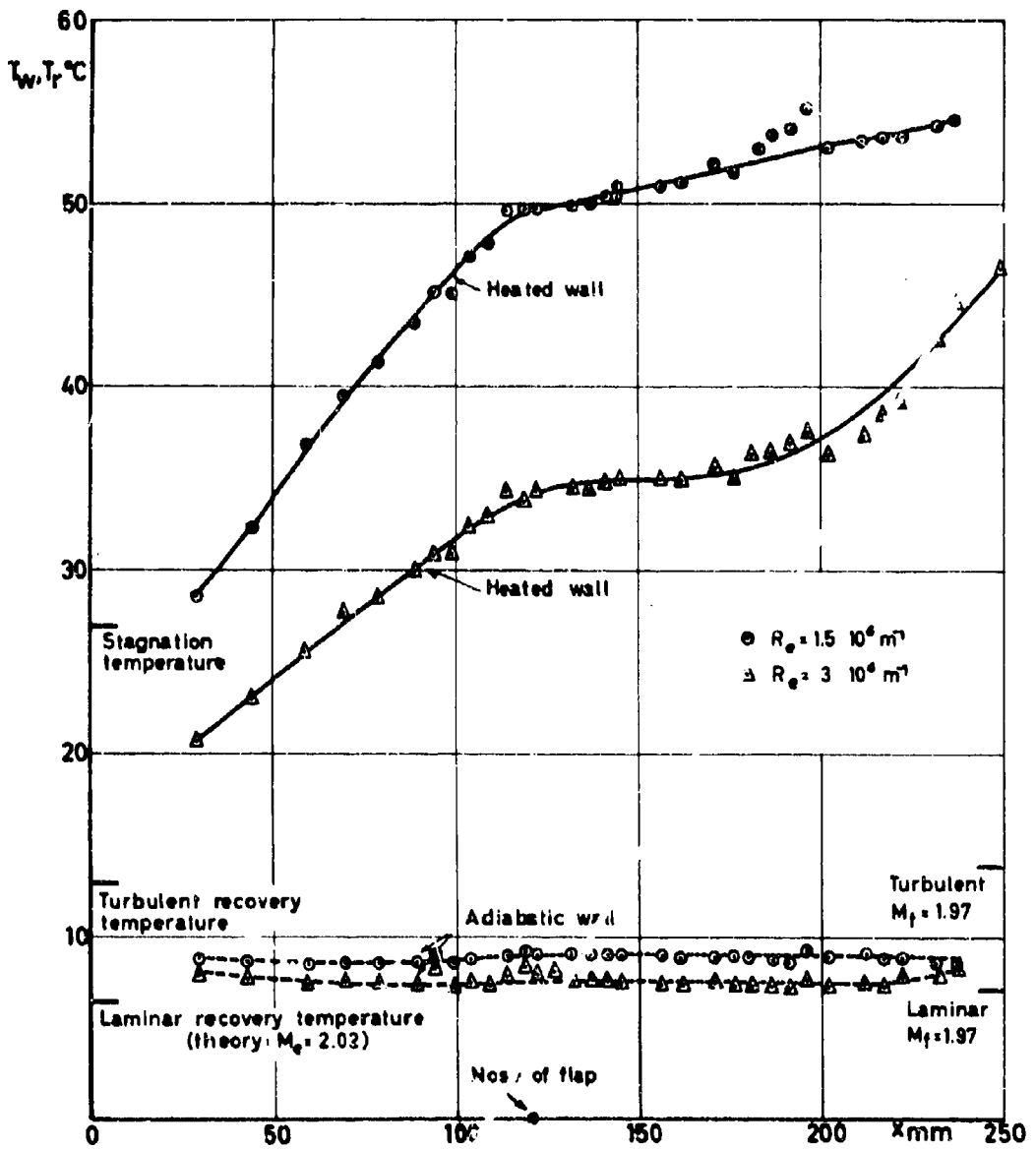

Fig. 4a - TEMPERATURE DISTRIBUTIONS FOR A FLAP ANGLE OF 1.5 deg.

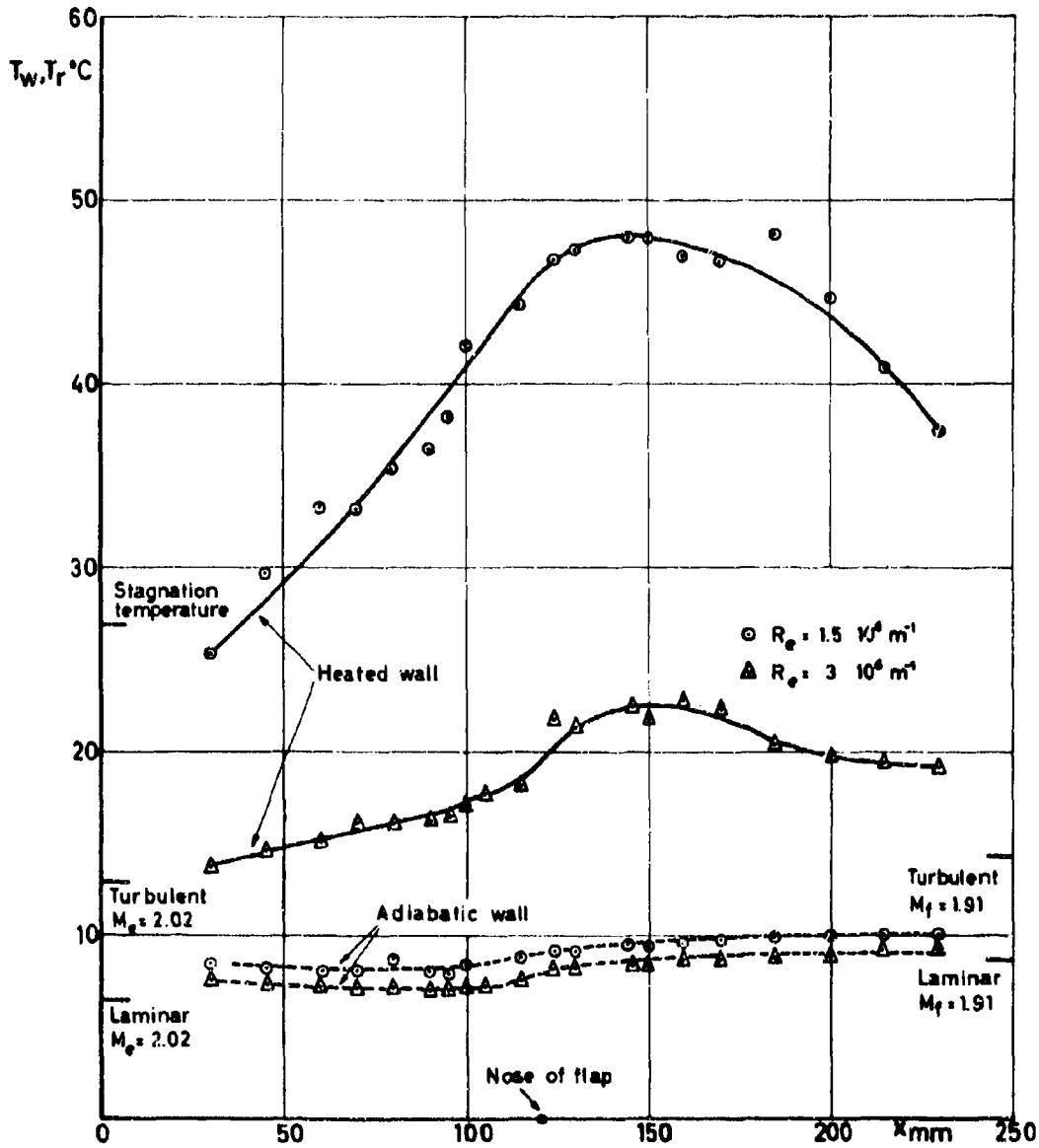

Fig. 4b- TEMPERATURE DISTRIBUTIONS FOR A FLAP ANGLE OF 3 deg.

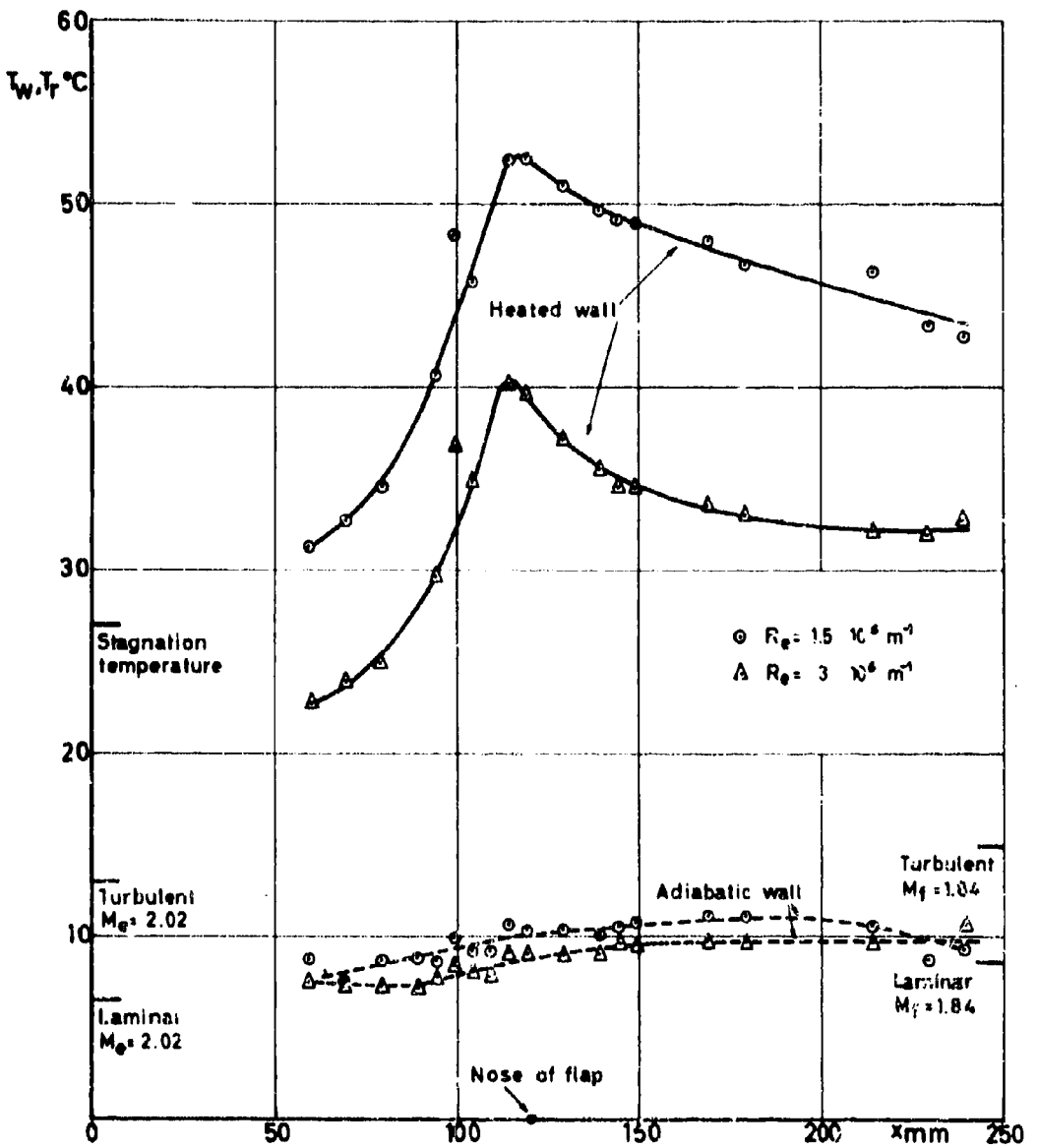

Fig. 4c - TEMPERATURE DISTRIBUTIONS FOR A FLAP ANGLE OF 5 deg.

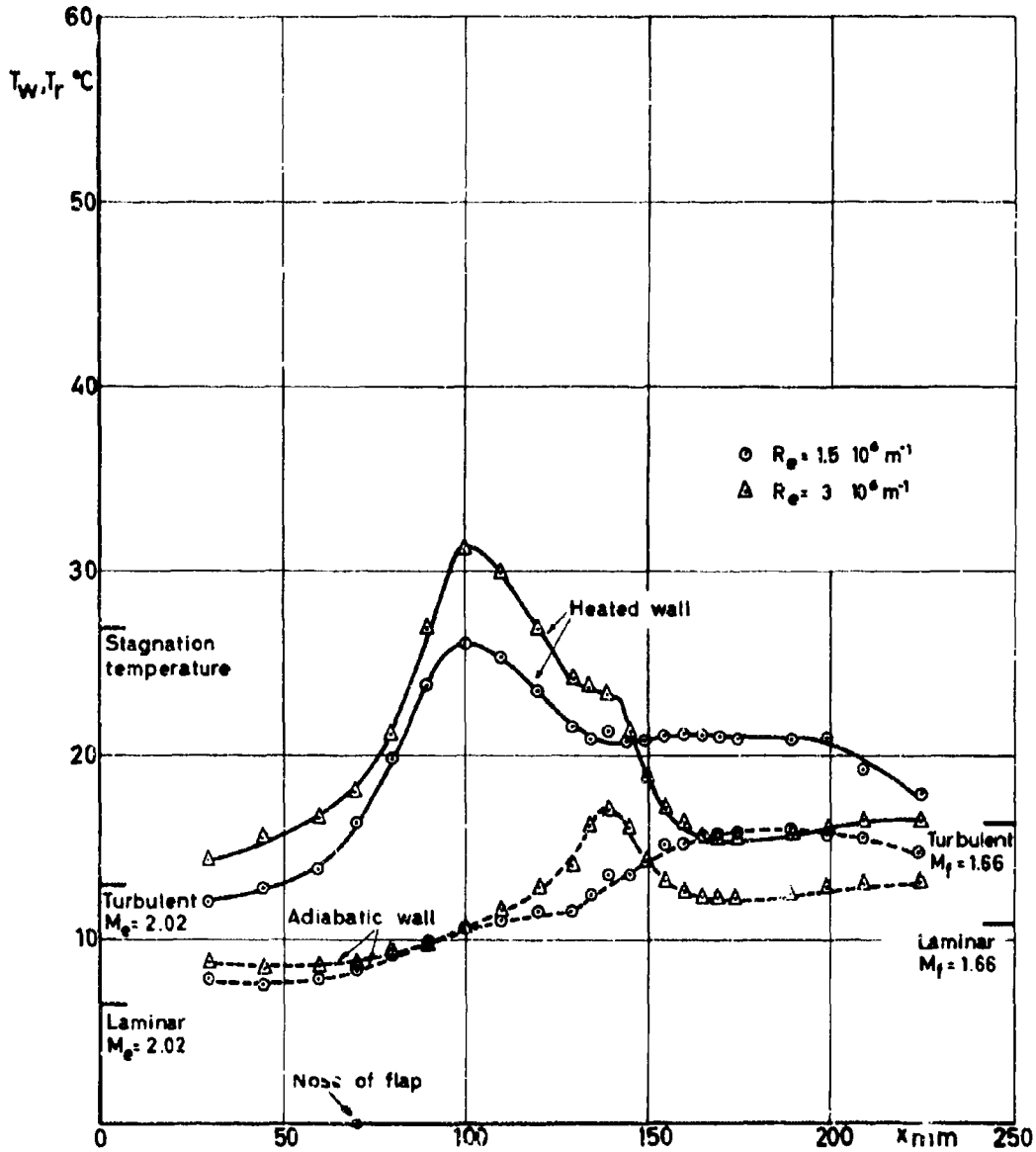

Fig. 4d - TEMPERATURE DISTRIBUTIONS FOR A FLAP ANGLE OF 10 deg.

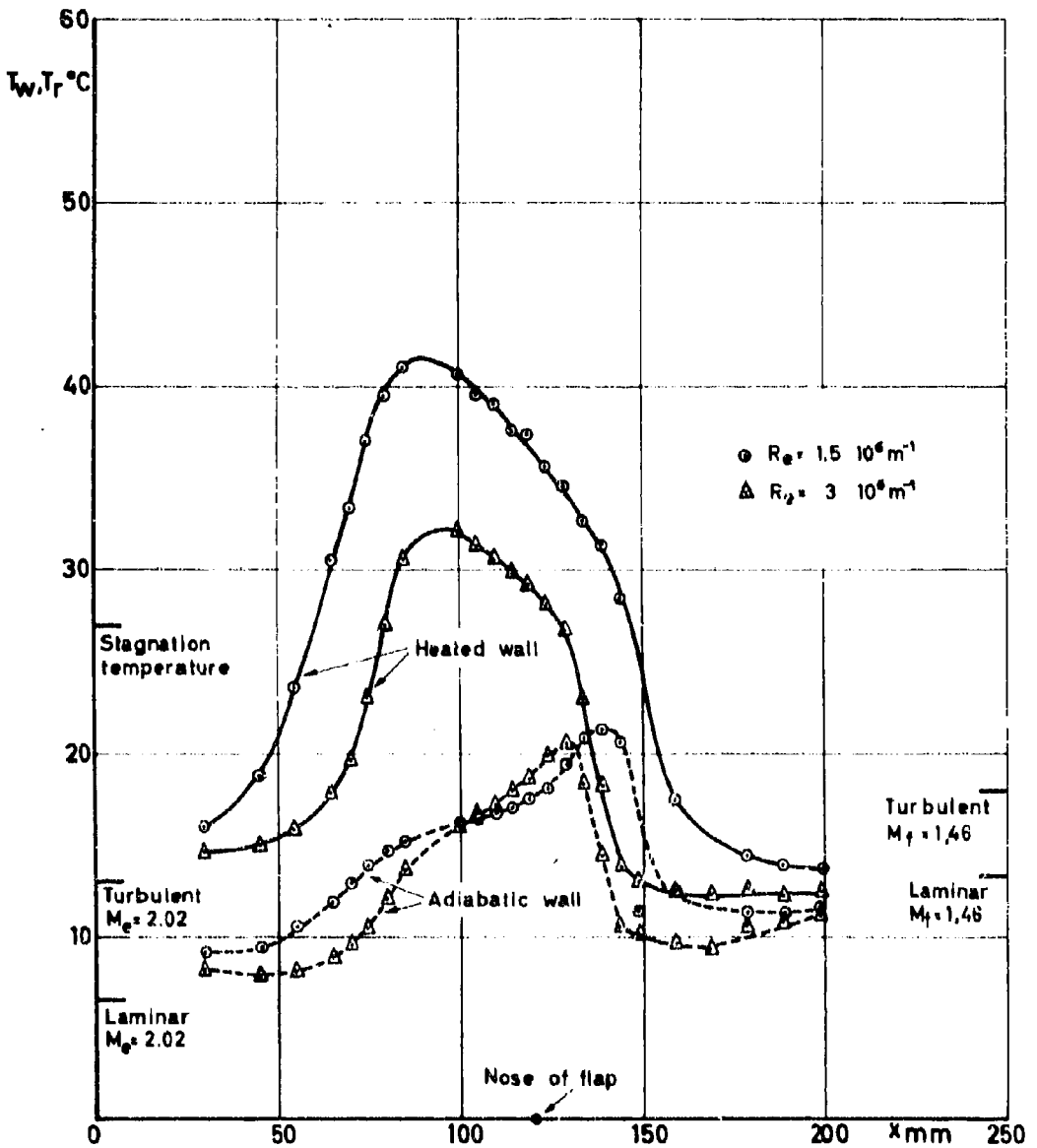

Fig. 6e - TEMPERATURE DISTRIBUTIONS FOR A FLAP ANGLE OF 15 deg.

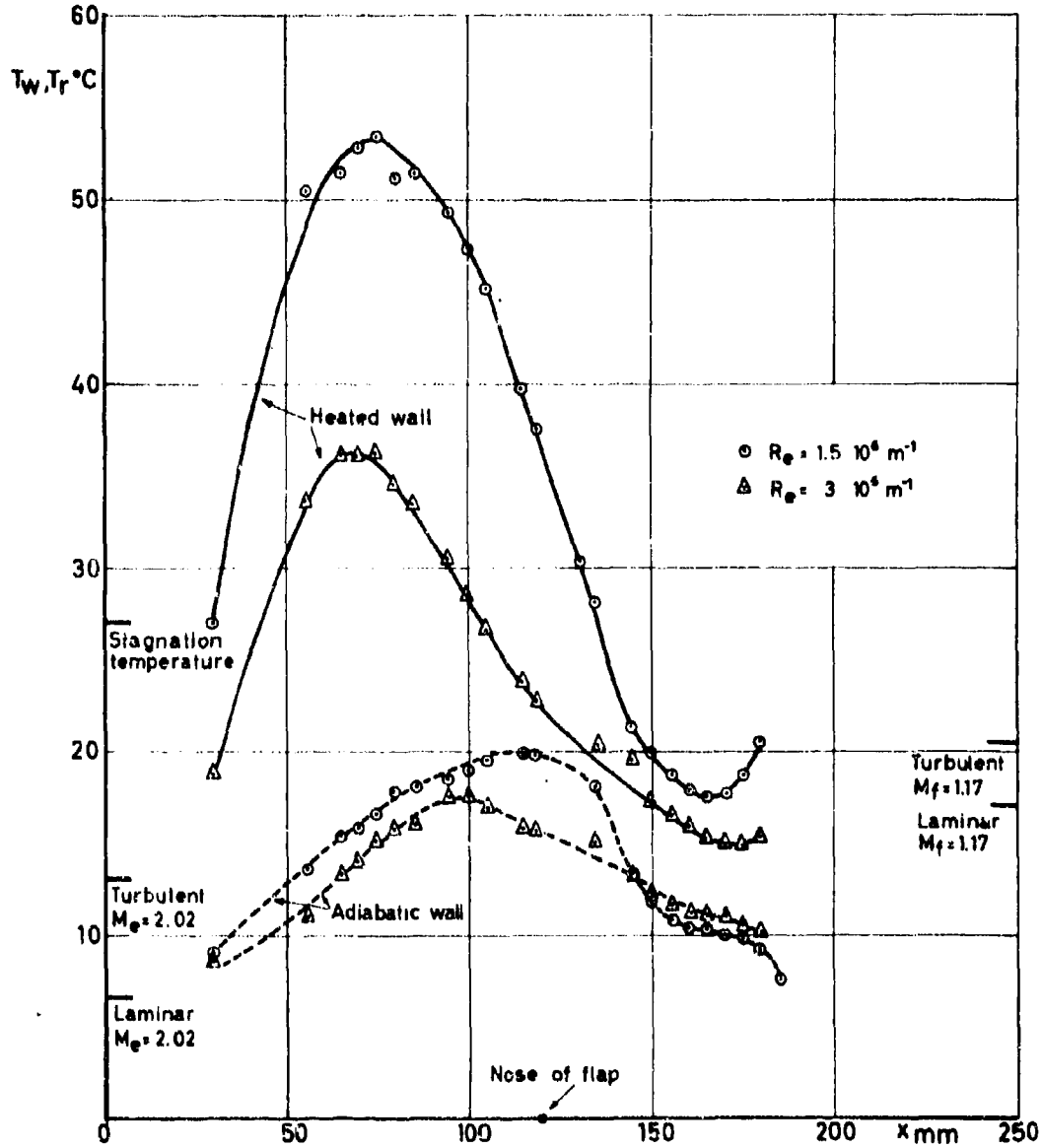

Fig. 4 f - TEMPERATURE DISTRIBUTIONS FOR A FLAP ANGLE OF 21 deg.

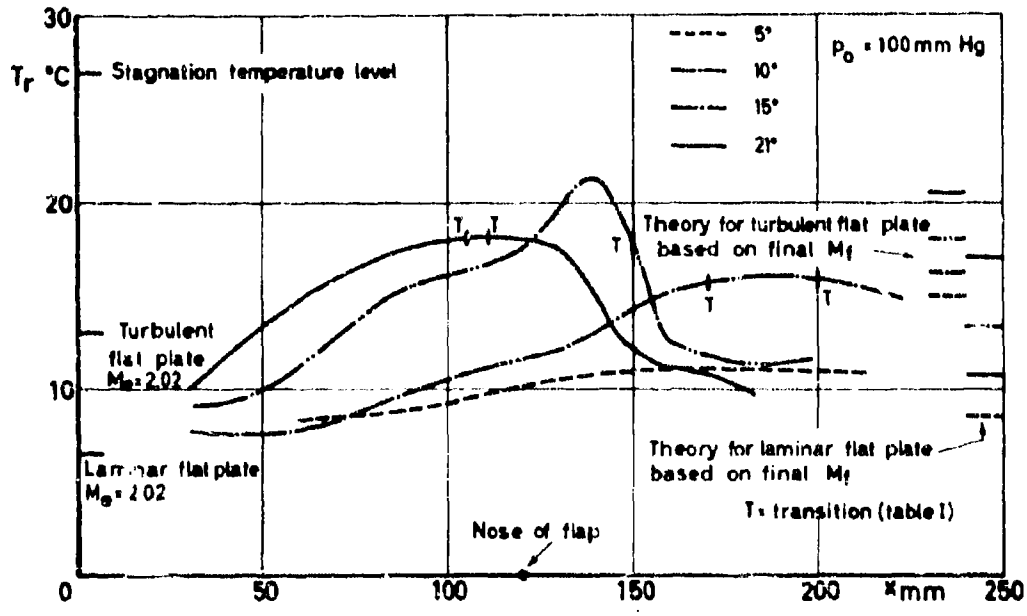

Fig.5a - SUMMARY OF THE RECOVERY TEMPERATURES FOR VARIOUS FLAP ANGLES - R_e=1.5 10^6 m^{-1}

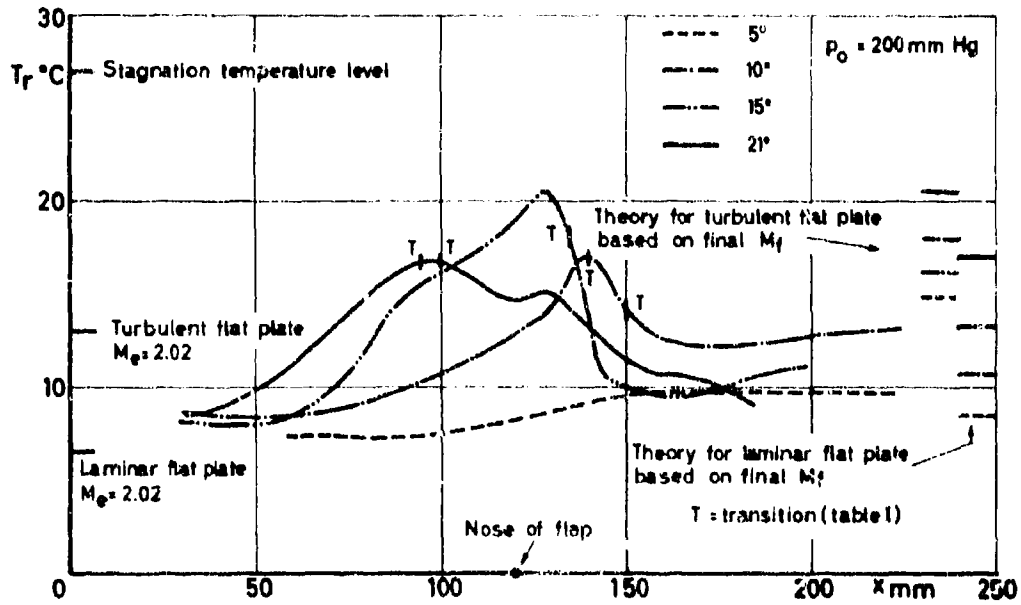

Fig. 5b - SUMMARY OF THE RECOVERY TEMPERATURES FOR VARIOUS FLAP ANGLES - R_e=3 10^6 m^{-1}

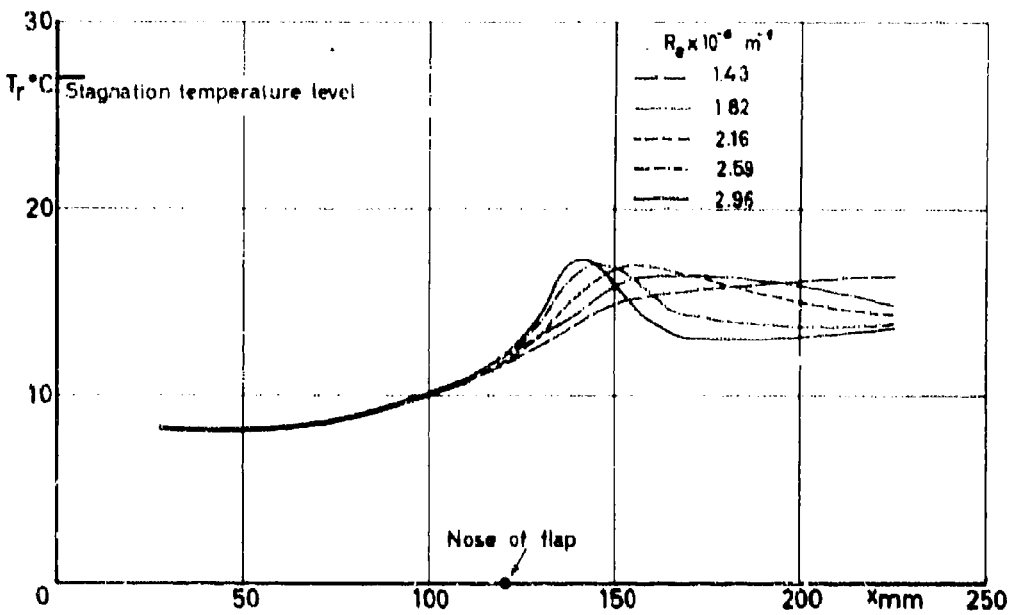

Fig. 6 - EFFECT OF UNIT REYNOLDS NUMBER ON RECOVERY TEMPERATURE DISTRIBUTION FOR A FLAP ANGLE OF 10 DEGREES.

a) $R_e = 1.5 \times 10^6\ m^{-1}$

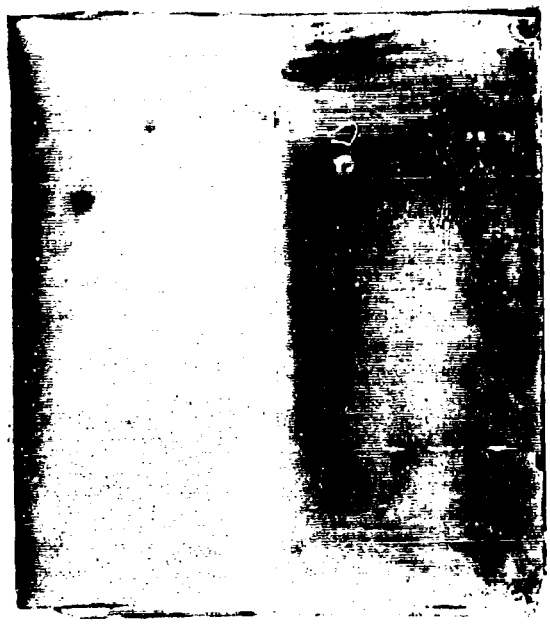

b) $R_e = 3.0 \times 10^6\ m^{-1}$

Fig. 7 - SUBLIMATION PICTURES OF THE FLOW AROUND A 10 deg. FLAP

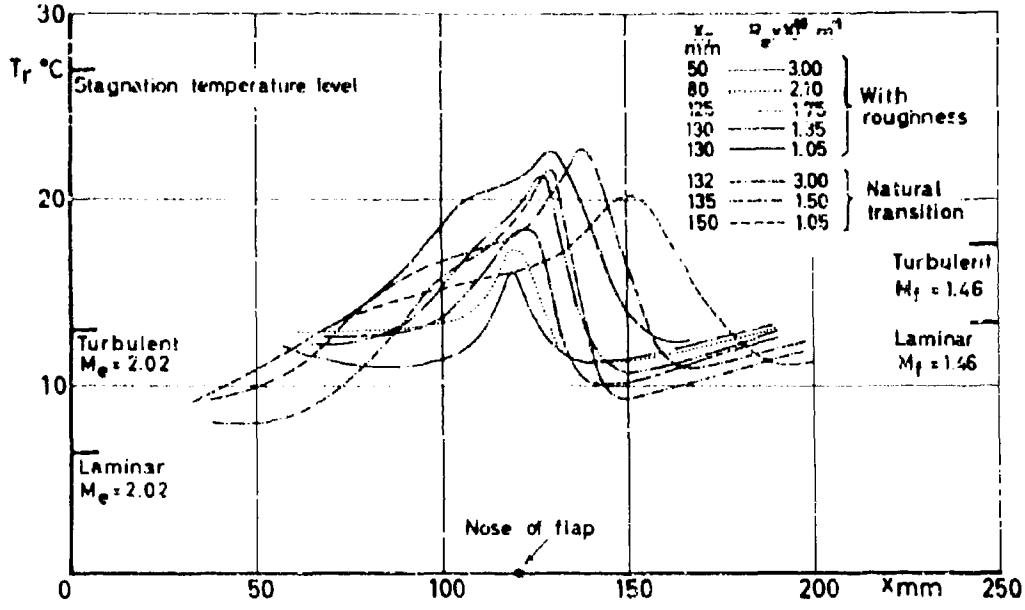

Fig.8 - EFFECT OF TRANSITION LOCATION ON THE RECOVERY TEMPERATURE DISTRIBUTION FOR A FLAP ANGLE OF 15 DEGREES.

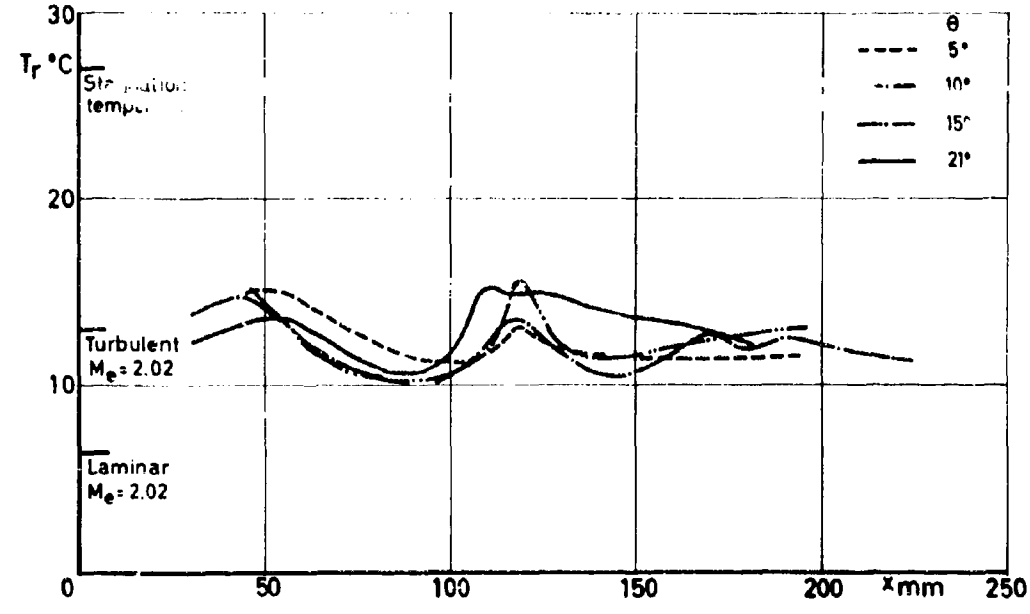

Fig.9 - RECOVERY TEMPERATURE DISTRIBUTIONS FOR FULLY TURBULENT FLOWS AT VARIOUS FLAP ANGLES.

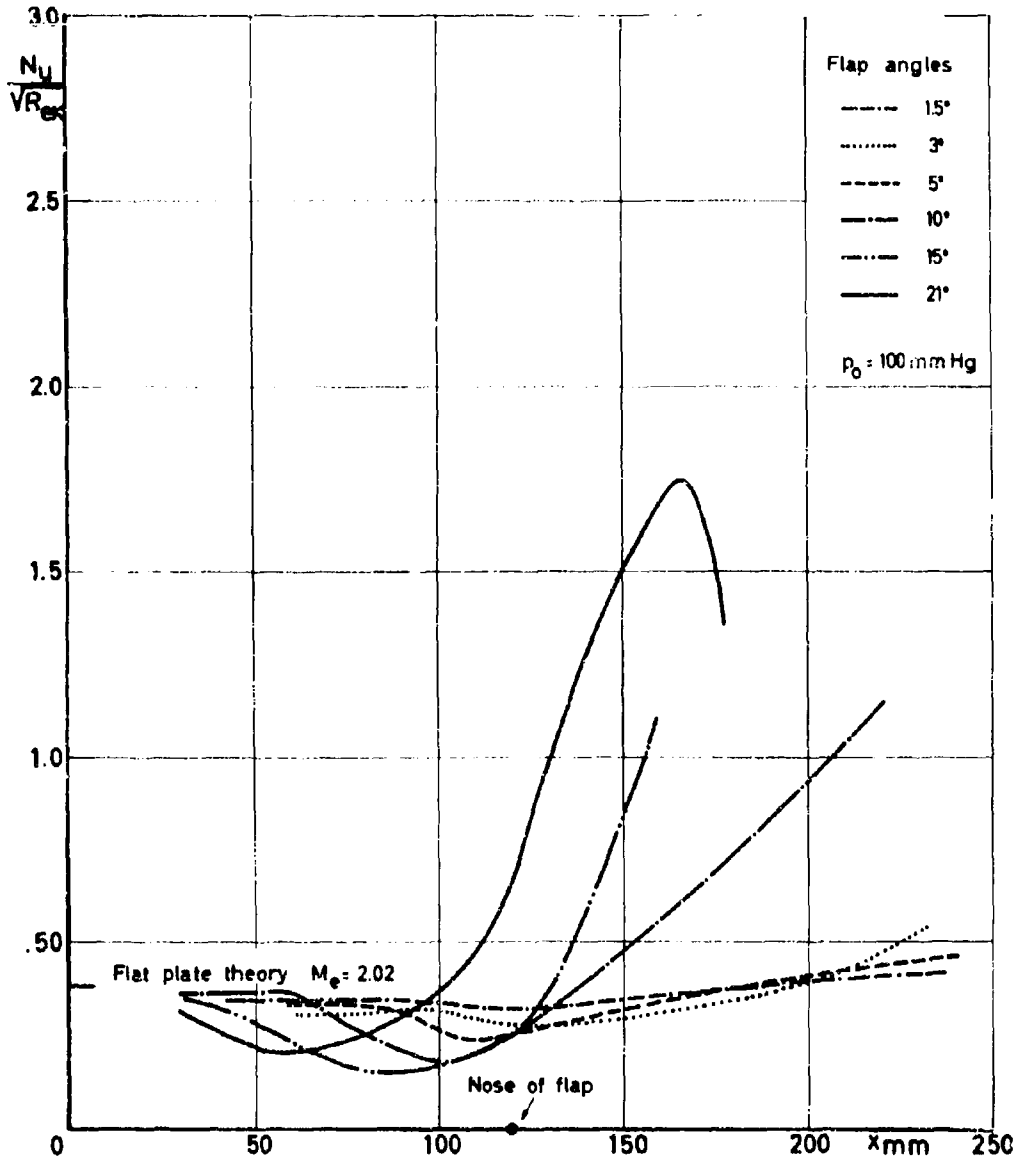

Fig. 10a - SUMMARY OF THE HEAT TRANSFER RESULTS FOR LAMINAR AND TRANSITIONAL FLOWS - R_e=1.5 $10^6 m^{-1}$

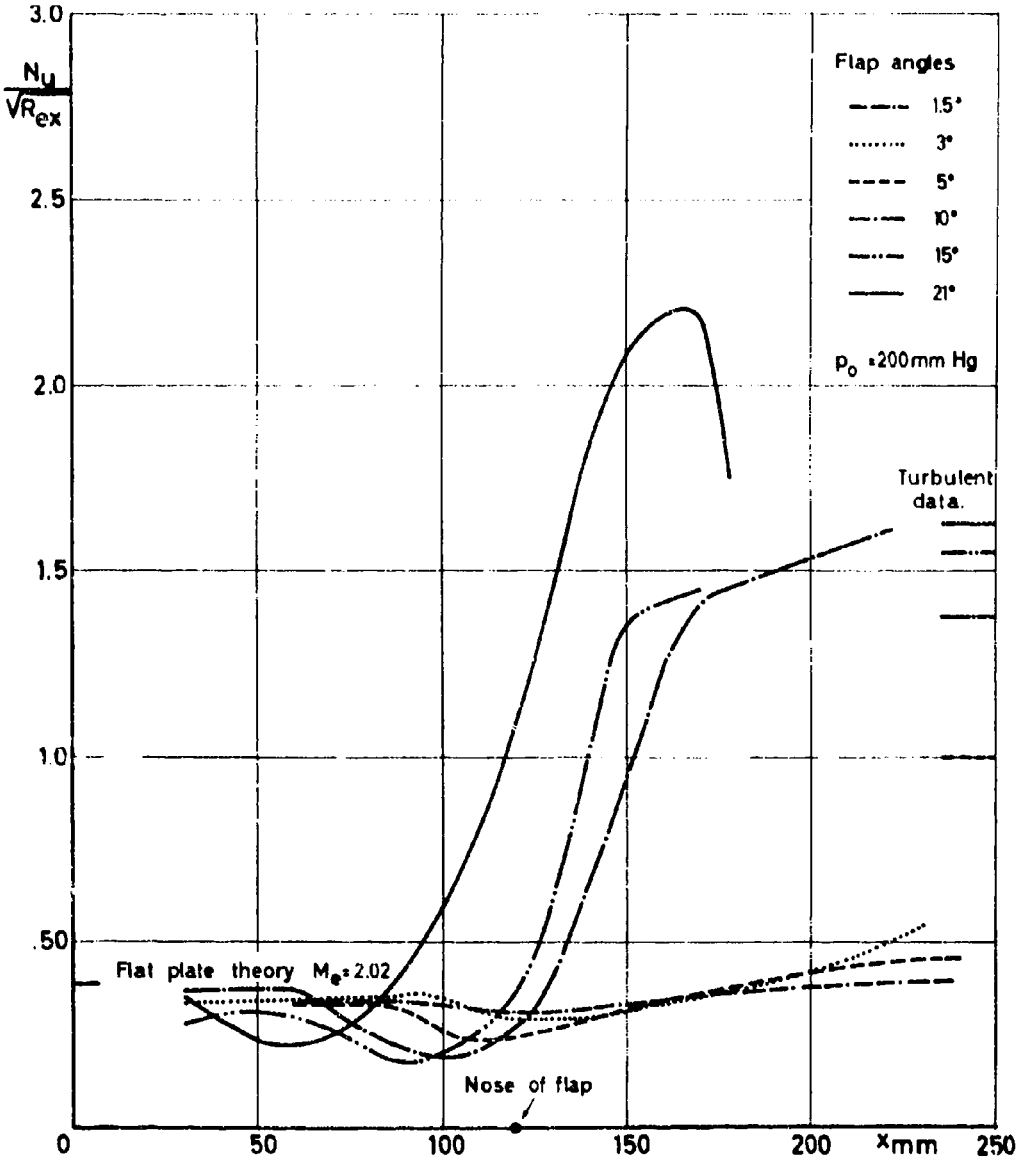

Fig. 10 b – SUMMARY OF THE HEAT TRANSFER RESULTS FOR LAMINAR AND TRANSITIONAL FLOWS – R_e=3 10^6 m^{-1}

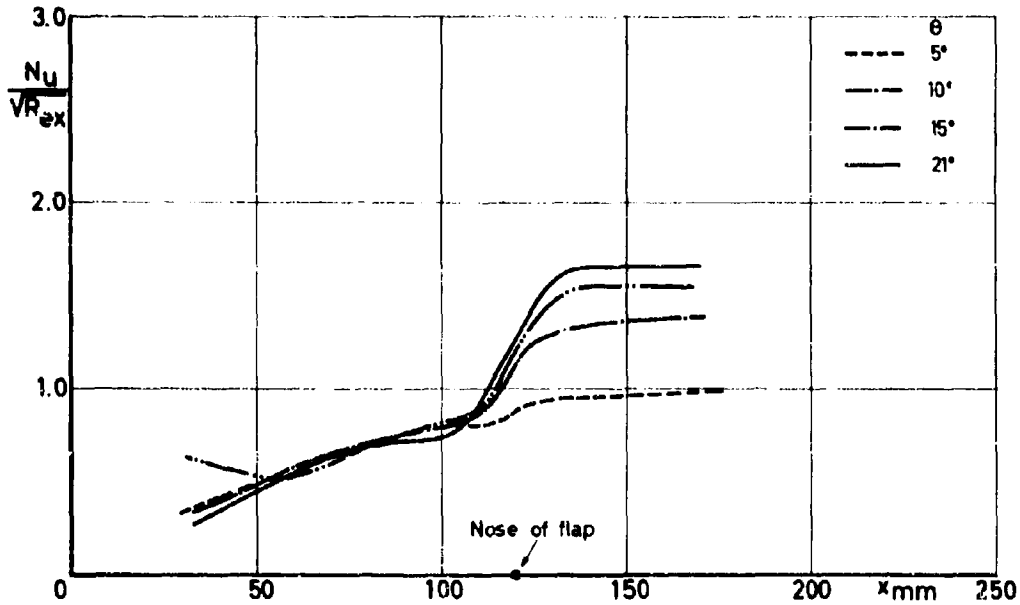

Fig.11 - SUMMARY OF THE HEAT TRANSFER RESULTS FOR TURBULENT FLOWS OVER FLAP MODELS.

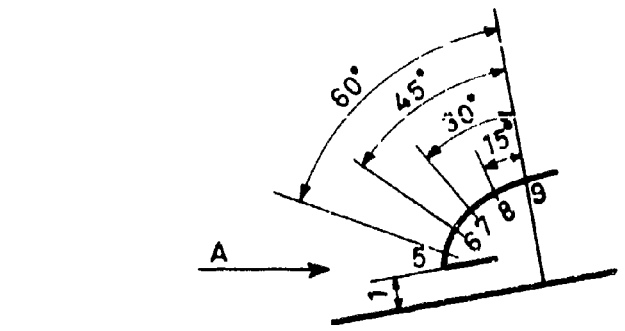

	x
3	- 5
9	+ 4
10	+ 7
11	+ 12
12	+ 17
13	+ 27
14	+ 42
15	+ 57

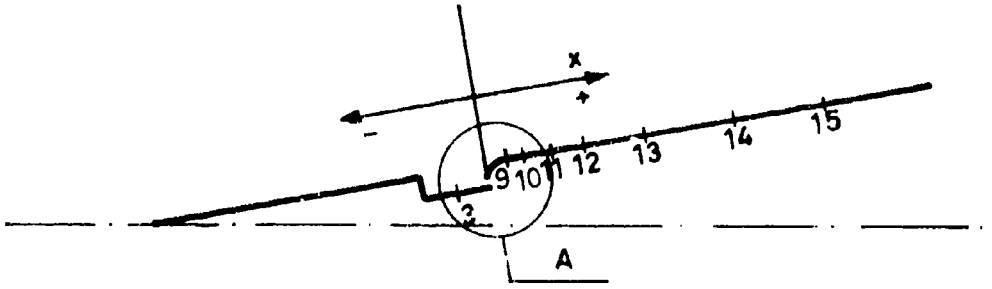

a) Location of the thermocouples

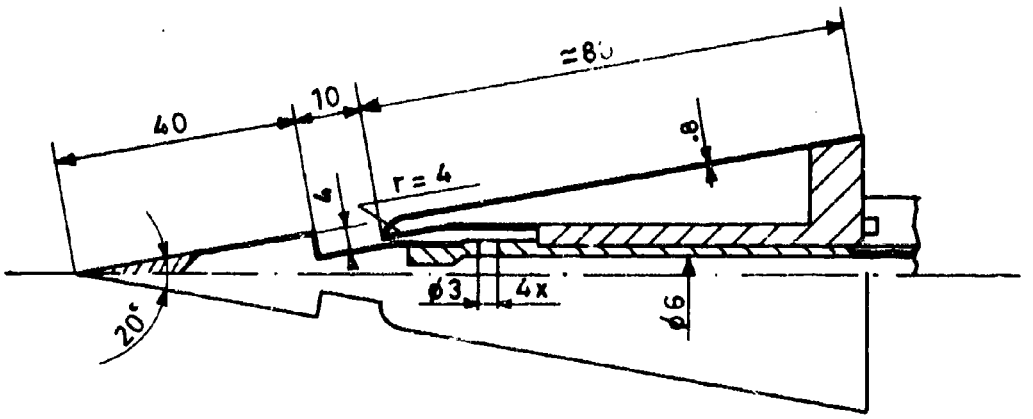

b) Section of the model

Figure 12 HEAT TRANSFER MODEL FOR HYPERSONIC TESTS

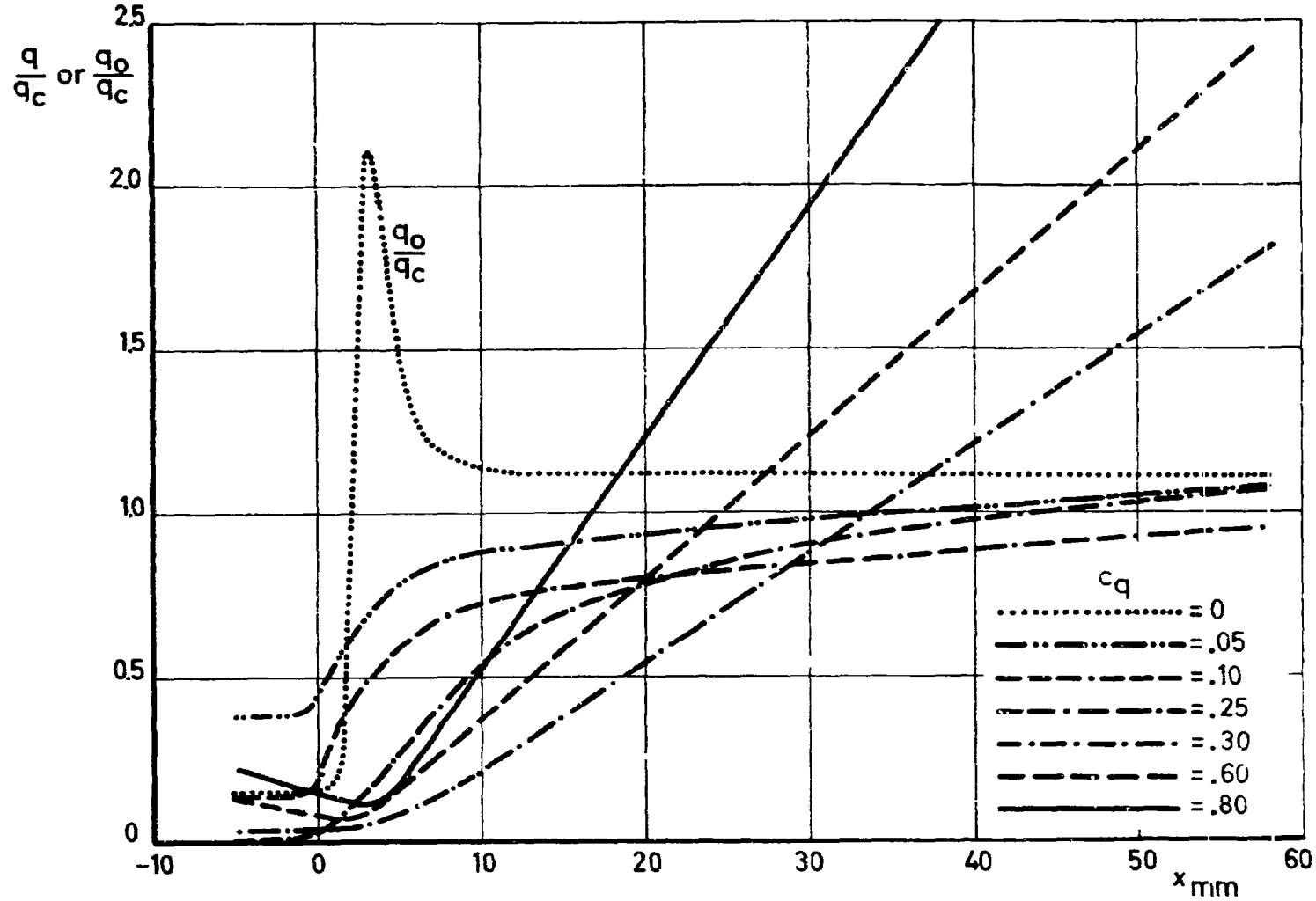

Figure 13 EFFECT OF MASS INJECTION ON HEAT TRANSFER DISTRIBUTION OVER A CONE-CAVITY MODEL AT M = 6.7
q_c: attached flow (cone); q_o: cavity without injection
q: cavity with injection

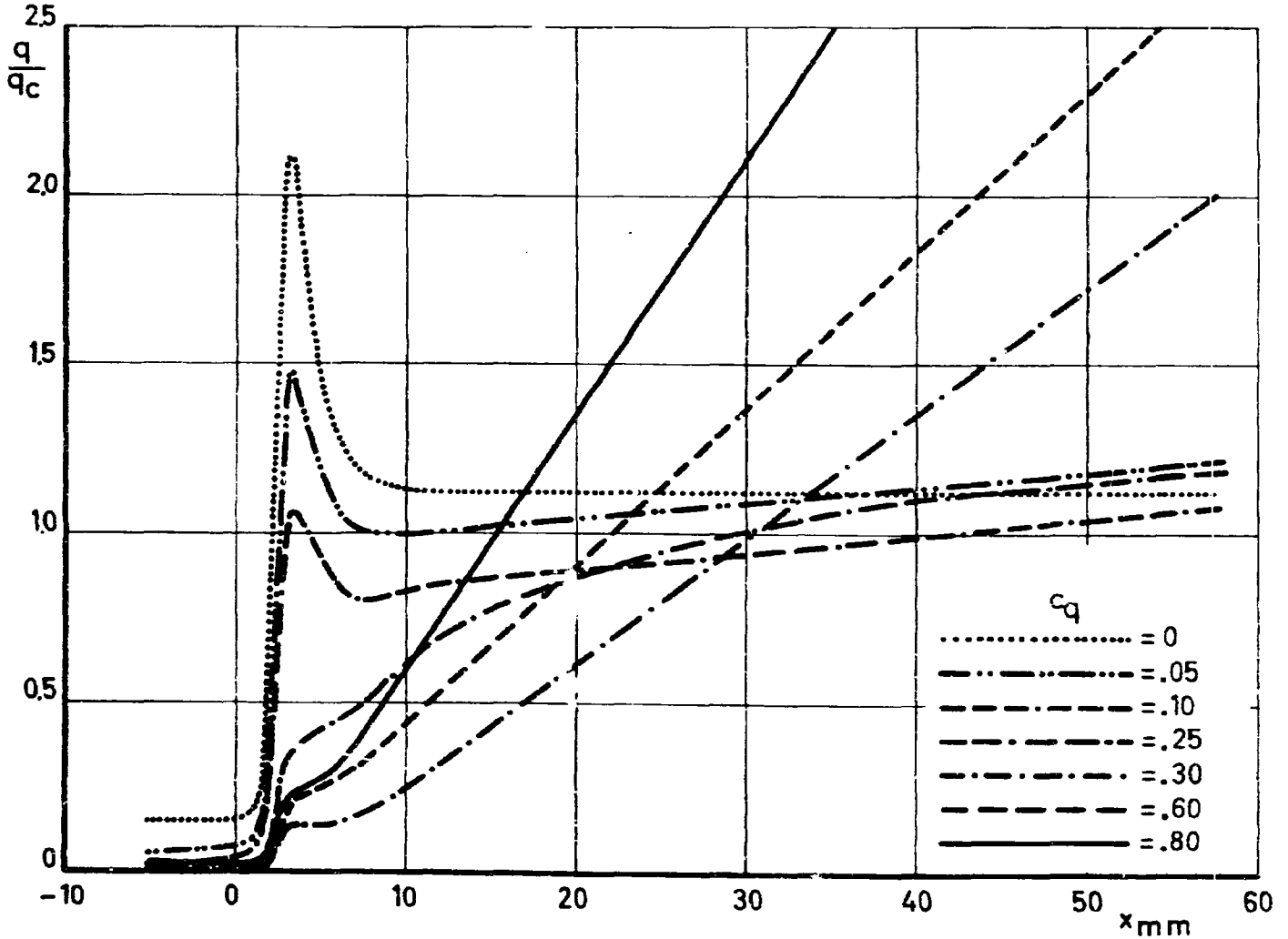

Figure 14 EFFECT OF MASS INJECTION ON HEAT TRANSFER DISTRIBUTION OVER A CONE CAVITY MODEL AT M = 6.7
q_c: attached flow (cone);
q: cavity with injection

Security Classification

DOCUMENT CONTROL DATA - R & D

(Security classification of title, body of abstract and indexing annotation must be entered when the overall report is classified)

1. ORIGINATING ACTIVITY (Corporate author)

Von Karman Institute for Fluid Dynamics
Aeronautic Laboratory
Rhode-Saint-Genese, Belgium

2a. REPORT SECURITY CLASSIFICATION

UNCLASSIFIED

2b. GROUP

3. REPORT TITLE

LAMINAR SEPARATION IN SUPERSONIC AND HYPERSONIC FLOWS

4. DESCRIPTIVE NOTES (Type of report and inclusive dates)

Scientific Final

5. AUTHOR(S) (First name, middle initial, last name)

Jean J. Gilsonn

6. REPORT DATE

30 September 1966

7a. TOTAL NO. OF PAGES

64

7b. NO. OF REFS

21

8a. CONTRACT OR GRANT NO.

AF-EOAR-66-6

8b. PROJECT NO. 9781-02

8c. 61445014

8d. 681307

9a. ORIGINATOR'S REPORT NUMBER(S)

9b. OTHER REPORT NO(S) (Any other numbers that may be assigned this report)

10. DISTRIBUTION STATEMENT

1. Distribution of this document is unlimited

11. SUPPLEMENTARY NOTES

TECH, OTHER

12. SPONSORING MILITARY ACTIVITY

AF Office of Scientific Research (SREM)
1400 Wilson Boulevard
Arlington, Virginia 22209

13. ABSTRACT

The static pressure, recovery temperature and heat transfer distribution have been measured on flat plates with flaps at a Mach number of 2.01. A uniform amount of heat was dissipated at the surface of the models. The angle of the flaps was varied between 1.5° and 21°. Laminar, transitional, and turbulent flows were considered. A large peak of recovery temperature existed, when transition was in the reattachment zone. Heat transfer distributions have been measured at a Mach number of 6.7 on a cone-cavity model with air injection into the separated flow region. The effect of injection was to considerably reduce the heat transfer rate to the cavity floor and in the reattachment region of the flow.

DD FORM 1 NOV 65 1473

Security Classification

14 KEY WORDS	LINK A		LINK B		LINK C	
	ROLE	WT	ROLE	WT	ROLE	WT
Hypersonic and Supersonic Flows Laminar Separation Mass Injection Cooling						